4-22-2014 12:00 AM

The hydrodynamic behavior of an inverse liquid-solid circulating fluidized bed

Amin Jaberi, *The University of Western Ontario*

Supervisor: Jesse Zhu, *The University of Western Ontario*

A thesis submitted in partial fulfillment of the requirements for the Master of Engineering Science degree in Chemical and Biochemical Engineering

The hydrodynamic behavior of an inverse liquid-solid circulating fluidized bed

(Thesis format: Integrated Article)

by

Amin Jaberi

Graduate Program in Chemical and Biochemical Engineering

A thesis submitted in partial fulfillment
of the requirements for the degree of
Master of Engineering Science

The School of Graduate and Postdoctoral Studies
The University of Western Ontario
London, Ontario, Canada

Abstract

In this work the hydrodynamic behavior of an inverse liquid-solid circulating fluidized bed (ILSCFB) system was studied. In addition, the hydrodynamic characteristic of the inverse liquid-solid fluidization under the conventional fluidization regime was also studied. The system consists of a downer with an inner column diameter of 7.6 cm and a height of 5.4 meters, an upcomer (riser) with an inner column diameter of 20 cm, a separator, and feeding and returning pipes which connect the downer and the upcomer. Based on the axial hydrodynamic behavior of the ILSCFB, it was found that the axial solids holdup in the downer is uniform. Similar to the heavy-particle LSCFB, the circulating fluidization regime in the downer was separated into the two zones including the initial circulating fluidization zone and the fully developed circulating fluidized zone as a function of the total liquid velocity in the downer. The effects of the solids inventory and the counter current flow in the upcomer on the hydrodynamics of the downer were also studied. Afterwards, the radial distribution of particles was studied in the downer of the ILSCFB. Interestingly, the radial structure of the two-phase flow was completely different from the case of the heavy-particle LSCFB. It was found that the solids holdup was greater in the center than near the wall of the downer. Finally, the conventional (non-circulating) inverse liquid-solid fluidization was studied in a column with a large diameter for the first time. The minimum fluidization velocity was obtained experimentally and compared with the Richardson and Zaki model. It was concluded that the Richardson and Zaki model can predict the bed expansion in the case of the inverse liquid-solid fluidization when the terminal velocity was calculated by the model of free rising light particles.

Keywords

Inverse liquid-solid circulating fluidized bed (ILSCFB), axial solids holdup, solids circulation rate, liquid velocity, radial distribution of particles, conventional fluidization regime

Acknowledgments

I would like to express my gratitude and appreciation to all those who gave me the possibility to complete this report.

I take this opportunity to express my profound gratitude and deep regards to my supervisor Professor Jesse Zhu for his exemplary guidance, monitoring and constant encouragement throughout the course of this thesis. The blessing, help and guidance given by him time to time shall carry me a long way in the journey of life on which I am about to embark.

The completion of this project could not have been accomplished without the support of my co-supervisor, Professor Dimitre Karamanev. I offer my sincere appreciation for the learning opportunities provided by him.

Special thanks go to support staff members of our group Jianzhang Wen and Hanning Li to help me to modify and design the experimental equipment. In addition, many thanks to George Zhang for his service

Last but not least, many thanks go to Tian Nan who helped me to carry out the experiments and gave suggestion in different parts.

Thanks are also extended to my friends, Ha Doan, Chengxiu Wang, Long Song, Vahid Vajihinejad, Cristina Salome Lugo, Stanislav Ivanov, Arash Mozaffari and Hojat Seyedy, who have always been helping and supporting me in the academic and daily life.

Lastly, I thank almighty, my parents and my brother for their constant encouragement without which this assignment would not be possible.

Co-Authorship Statement

Title: The Axial Hydrodynamic Behavior of Light Particles in an Inverse Liquid-Solid Circulating Fluidized Bed

Author: Amin Jaberi, Jesse Zhu, Dimitre Karamanev

All the experiments were carried out by Amin Jaberi under the gaudiness of the advisors Jesse Zhu and Dimitre Karamanev. All drafts of this manuscript were written by Amin Jaberi. Modifications were completed under the supervision of advisors Jesse Zhu and Dimitre Karamanev. The final version of this manuscript is ready for submission.

Title: Radial Distribution of Light Particles in an Inverse Liquid-Solid Circulating Fluidized Bed

Author: Amin Jaberi, Dimitre Karamanev, Jesse Zhu, Tian Nan

All portions of the experiments were carried out by Amin Jaberi with the assistance of Tian Nan. All drafts of this manuscript were written by Amin Jaberi. Modifications were completed under the supervision of advisors Dimitere Karamanev and Jesse Zhu. The final version of this manuscript is ready for submission.

Table of Contents

List of Tables

List of Figures

List of Appendices

Chapter 1

1 General Introduction

1.1 Introduction

Inverse/upward liquid-solid fluidization refers to a two-phase system where particles with density lower/higher than liquid density are suspended by a stream of liquid flowing in the opposite direction to buoyancy/gravity. In upward liquid-solid systems, particles density is higher than liquid density. Thus, the fixed bed of particles at the bottom of the fluidized column is fluidized when an upward liquid stream is uniformly distributed into the fixed bed. Therefore, the drag force counters the gravitational force at liquid velocity beyond the minimum fluidization velocity of particles. In contrast, when the density of particles is lower than the liquid density, particles tend to stay at the top of the fluidized column. In this case, fluidization is obtained by a downward flow of the liquid and consequently drag force counters the buoyancy force at liquid velocity beyond the minimum fluidization velocity.

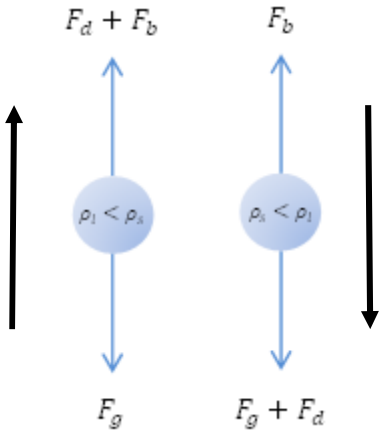

Figure 1-1: Left: upward fluidization, Right: downward (inverse) fluidization

In a downward or inverse fluidization, at a liquid velocity below the minimum fluidization velocity, particles remain in a fixed state at the top of the fluidized column known as the downer. When liquid velocity increases beyond the minimum fluidization velocity, the fluidization of particles is obtained and the liquid-solid system enters the

conventional fluidization regime. In this regime of fluidization, there is a clear boundary between the dense region of the particles at the top and the bottom freeboard which is occupied by liquid [1]. Further increasing the liquid flowrate in the downer causes this clear boundary to disappear and a more dilute mass of particles in the liquid is observed. By further increasing the liquid velocity beyond the terminal rising velocity, particles are transported out of the column [2, 3]. Under this condition, particles are carried out of the downer by the downward liquid stream. If particles are separated at the bottom of the downer and stored in another column, particles recirculation can be achieved between the two columns by continuously feeding particles to the top of the downer from the second column.

This idea resulted in designing the novel two-phase system named "Inverse Liquid-Solid Circulating Fluidized Bed", by Sang [4].

Generally fluidized bed reactors known as dense fluidized bed reactors have been used in a wide range of applications. Interestingly, in the case of liquid-solid fluidization, some biotechnological processes such as an aerobic wastewater treatment [5, 6], and ferrous iron oxidation [7] in inverse fluidized bed biofilm reactors have demonstrated that inverse fluidized bed bioreactors are more efficient in comparison to upflow fluidized bed reactors. In addition, studies about the hydrodynamic behavior of the inverse liquid-solid fluidization for example hydrodynamic characteristics of inverse liquid-solid fluidization [8], bed expansion of inverse liquid-solid fluidization [9], and Newton’s law for free rising spheres [10] have shown that in some parts hydrodynamic behavior of the inverse liquid-solid fluidization is different from the upward one and further research in this area is still necessary.

On the other hand, it was found that a type of fluidized bed reactor, circulating fluidized bed (CFB), has more advantages rather than dense phase fluidized bed reactors [1]. It was concluded that operation of the CFB at high velocity increases the contact between the particles and the fluid [1]. On this basis, application of upward liquid-solid circulating fluidized bed (LSCFB) reactors has become an appropriate choice in different areas such

as waste water treatment [11] and continuous recovery of proteins from unclarified whole broth [12].

In the last two decades, comprehensive hydrodynamic studies of upward LSCFB reactors for instance radial distribution of particles [13], radial distribution of the liquid velocity [14], axial hydrodynamic behavior of the LSCFB [2], and the onset velocity of the LSCFB [15] have been carried out. These works can set a proper pattern to study the hydrodynamic behavior of the inverse liquid-solid circulating fluidized bed.

1.2 Objectives

The primary steps to understand capabilities of the inverse liquid-solid circulating fluidized bed reactor are to study the hydrodynamic behavior of this reactor. On this basis, the main objectives of this work are

1- To conduct a study on the axial hydrodynamic of the inverse LSCFB including solids circulation rate and particles distribution in the downer.
2- To observe the effects of some factors such as solids inventory and counter current flow in the riser or upcomer on solids circulation rate and particles distribution in the downer.
3- To employ the proper techniques to measure the radial phase distribution.
4- To study the radial flow structure in the downer under the circulating fluidization regime.
5- To compare the hydrodynamic behavior of the inverse and upward LSCFB.
6- To investigate the inverse liquid-solid fluidization under the conventional fluidization regime in a column with a large diameter.

1.3 Thesis Structures

Based on the objectives, this thesis includes the following chapters:

Chapter 1 contains a simple definition of the upward and inverse liquid-solid fluidization and is followed by a general literature review.

Chapter 2 describes the experimental setup and different techniques of measurements applied in this study.

Chapter 3 reports the axial hydrodynamic behavior of the inverse LSCFB. In this chapter, the solids circulation rate and the average solids holdup under a wide range of operating conditions in the downer are discussed and compared to the results for the upward LSCFB. Later, the effects of different factors such as solids inventory and counter current flow in the riser or upcomer on the downer hydrodynamics are studied.

Chapter 4 shows the results of the experimental study of the radial flow structure of the inverse LSCFB. Three measurement techniques were employed and the current results are compared with previous results obtained for the upward LSCFB reactor containing particles with density higher than liquid density.

Chapter 5 presents the results of the study of the pressure drop and bed expansion in the riser or upcomer with a larger diameter. The minimum fluidization velocity is measured and different equations are presented to predict the minimum fluidization velocity.

Chapter 6 summarizes the conclusions obtained in the above studies and gives recommendations for future research.

References

[1] Zhu, J.-X., D. G. Karamanev, A. S. Bassi and Y. Zheng (2000). "(Gas-) liquid-solid circulating fluidized beds and their potential applications to bioreactor engineering". The Canadian Journal of Chemical Engineering 78(1): 82-94.

[2] Zheng, Y., J.-X. Zhu, J. Wen, S. A. Martin, A. S. Bassi and A. Margaritis (1999). "The axial hydrodynamic behavior in a liquid-solid circulating fluidized bed". Canadian Journal of Chemical Engineering 51(50): 16242-16250

[3] Liang, W., S. Zhang, J.-X. Zhu, Y. Jin, Z. Yu and Z. Wang (1997). "Flow characteristics of the liquid-solid circulating fluidized bed". Powder Technology 90(2): 95-102.

[4] Long Sang (2013). "Particle Fluidization in Upward and Inverse Liquid-Solid Circulating Fluidized Bed". The University of Western Ontario, PhD Thesis.

[5] Nikolov, L., D. Karamanev, T. Penev, and D. Dimitrov (1990). "Full-Scale Inverse Fluidized Bed Biofilm Reactor for Wastewater Treatment" 2nd Int. Biotechnol. Conf.: Asian-Pacific Biotechnol. Conf., 112, Seoul, Korea.

[6] Karamanev, D. G. and L. N. Nikolov (1996). "Application of inverse fluidization in wastewater treatment: From laboratory to full-scale bioreactor". Environmental Progress 15(3): 194-196.

[7] Karamanev, D. G., and L. N. Nikolov (1988). "Influence of Some Physicochemical Parameters on Bacterial Activity of Biofilm". Biotechnol. Bioeng. 31(4): 295-299

[8] Fan, L.-S., K. Muroyama and S. H. Chern (1982). "Hydrodynamic Characteristics of Inverse Fluidization in Liquid-Solid and Gas-Liquid-Solid Systems". The Chemical Engineering Journal 24(2): 143-150.

[9] Karamanev, D.G., Nikolov, L.N., (1992b). "Bed expansion of liquid–solid inverse fluidization". AICHE Journal 38(12): 1916-1922

[10] Karamanev, D.G., Nikolov, L.N., (1992a). "Free rising spheres do not obey Newton's law for free settling". AICHE Journal 38 (11), 1843–1846.

[11] Chowdhury, N., J. Zhu, G. Nakhla, A. Patel and M. Islam (2009). "A novel liquid-solid circulating fluidized-bed bioreactor for biological nutrient removal from municipal wastewater". Chemical Engineering and Technology 32(3): 364-372.

[12] Lan, Q., J. X. Zhu, A. S. Bassi, A. Margaritis, Y. Zheng and G. E. Rowe (2001). "Continuous protein recovery using a liquid-solid circulating fluidized bed ion exchange system: Modelling and experimental studies". Canadian Journal of Chemical Engineering 79(4): 687-687.

[13] Razzak, S. A., S. Barghi, J.-X. Zhu (2009). "Application of electrical resistance tomography on liquid–solid two-phase flow characterization in an LSCFB riser". Chemical Engineering Science 64(12): 2851-2858

[14] Zheng, Y., Zhu, J.-X. (2003). "Radial distribution of liquid velocity in a liquid–solid circulating fluidized bed". International Journal of Chemical Reactor Engineering 1, Article Number: S1.

[15] Zheng, Y. and J.-X. Zhu (2001). "The onset velocity of a liquid-solid circulating fluidized bed". Powder Technology 114(1-3): 244-251.

Chapter 2

2 Experimental Apparatus and Measurement Techniques

2.1 Inverse liquid-solid circulating fluidized bed

A schematic diagram of the inverse liquid-solid circulating fluidized bed (ILSCFB) reactor used in this study is shown in Figure 2-1. The reactor downer was operated at a liquid superficial velocity higher than the particle terminal rising velocity. Therefore, it is essential to feed particles at the top of the downer and to separate the entrained particles from its bottom and recirculate them back to the top of the downer again.

The reactor consists of a Plexiglas downer with an inner column diameter of 7.6 cm and a height of 5.4 meters, a Plexiglas liquid-solid separator, a Plexiglas riser or upcomer with a diameter of 20 cm, and the solids return and feed pipe connecting the downer and upcomer. In this study, the solid phase was represented by spherical Styrofoam spheres with a mean diameter of 0.8 mm and density of 28 kg/m^3 while liquid phase was tap water. The density of the particles was measured with the fully automatic and accurate gas displacement pycnometer, "AccuPyc 1340".

At the top of the downer, main and auxiliary liquid distributors are installed to introduce the water into the downer. The main liquid distributor was made of seven stainless steel tubes occupying 19.5% of the downer area and extended 0.2 m down from the column top, and the auxiliary liquid distributor was made of a porous plate with 4.8% opening area at the top of the downer. The system also included two water tanks connected to each other as the source of the water for the entire system. From one tank water is pumped and divided into two streams leading to the main and auxiliary liquid distributors.

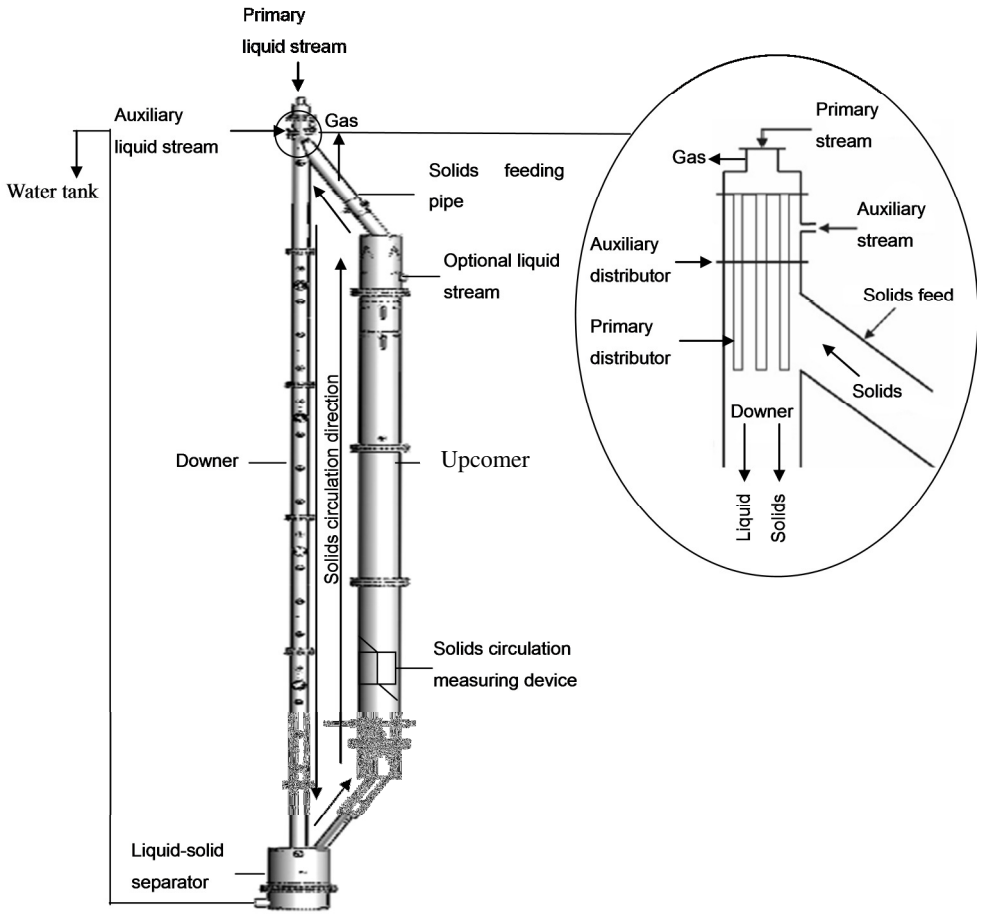

Figure 2-1: Schematic diagram of the inverse LSCFB reactor

(Sang [1])

When the total liquid velocity in the downer reaches the minimum fluidization velocity, particles move away from each other and the bed of the particles from the fix bed expands slowly in a downward direction. With a further increase of the superficial liquid velocity over the terminal velocity, particles begin to move out of the bed. Under this condition, particles are carried by the downward liquid flow and then at the bottom of the downer are separated from the liquid in a cylindrical liquid–solid separator. Liquid is returned to the liquid tank through the pipe which was designed as a Π - shape. The maximum height of this pipe is at the highest level of the reactor to ensure that the entire system is filled with water during the experiments. On the other hand, particles move from the separator to the upcomer through the pipe which connects the separator and upcomer. Particles move up in the upcomer because of their buoyancy and are stored at

the top of the upcomer. Then through the pipe connected from the top of the upcomer, particles feed into the top of the downer and recirculation of the particles completes in the reactor. The auxiliary liquid flow plays an important role in controlling the circulation of the particles. If auxiliary flow is set on zero, circulation of the particles is no longer occurring.

Periodically, water inside the tanks was refilled to prevent the accumulation of external substances which influence the hydrodynamic measurement. The temperature of the water was checked during experiments to make sure that all the experiments were performed under the same condition.

2.2 Measurement techniques

2.2.1 Solids circulation measuring device

In order to measure the superficial solids velocity in the downer, a devise named the solids circulation measuring device [2] was located near the bottom of the upcomer. The upcomer was divided into two equal sections with two half butterfly valves mounted at the top and the bottom of the two-half section. By properly flipping the two half butterfly valves from one side to the other, particles moving up in the upcomer can be accumulated on one side of the measuring section and increased further in the form of packed bed. A certain distance from the top of the valve where particles begin to accumulate is marked. Thus, the required time to fill that volume with particles is measured and the superficial solids velocity is calculated by the following equation:

$$U_s = \frac{h_s \left(\frac{A_r}{2}\right)\varepsilon_s}{tA_d} \tag{2.1}$$

where A_r and A_d are the areas of the upcomer and downer respectively, h is the accumulated height of particles in the measuring section and t is the accumulation time for the particles.

2.2.2 Manometers

In this study, manometers were used to measure the average solids holdup, pressure drop across the bed and bed expansion. Six ports at different heights were placed along both the downer and the upcomer. These ports were connected by tubes to a series of manometers. Table 2-1 shows the exact place of the pressure ports along both columns. Since the hydrostatic pressure at different heights of both columns was high, open-end manometers were not used in this experiment to prevent the overflowing of water in manometers. In this case, the ends of the manometers were connected to a tank full of air and the pressure of air inside the tank was controlled.

Table 2-1: Positions of the pressure ports on the axial direction

Distance from main liquid distributor (cm) **Downer (7.6 cm I.D.)**	Distance from liquid distributor (cm) **Upcomer (20 cm I.D.)**
111.4	8.4
187.4	37.9
238.4	73.4
289.4	109.4
366.4	144.4
416.4	179.4

Average solids holdup

As long as downer or upcomer is occupied only by water, the level of water inside the manometers was equal. Before each test, this level was checked to make sure that pressure ports were not blocked by particles or bubbles of air. But if the downer or upcomer contained both water and particles, due to the mixture density of particles and

water was lower than water density inside the manometers, water levels inside the manometers were different. Between the two manometers the pressure balance is governed by the following equation:

$$P_g + \rho_l h_m g + \rho_l g X_1 + [\rho_l(1-\varepsilon_s) + \rho_s \varepsilon_s] g \Delta h - \rho_l g \Delta h - \rho_l g X_1 - P_g = 0 \qquad (2.2)$$

By simplification of Equation (2.2), average solids holdup is obtained by the following equation:

$$\varepsilon_s = \frac{h_m}{\Delta h} \times \frac{\rho_l}{\rho_l - \rho_s} \qquad (2.3)$$

where h_m is the height difference between the levels of the water inside the manometers, Δh is the distance between the pressure ports, ρ_l and ρ_s are the liquid and the particles density respectively.

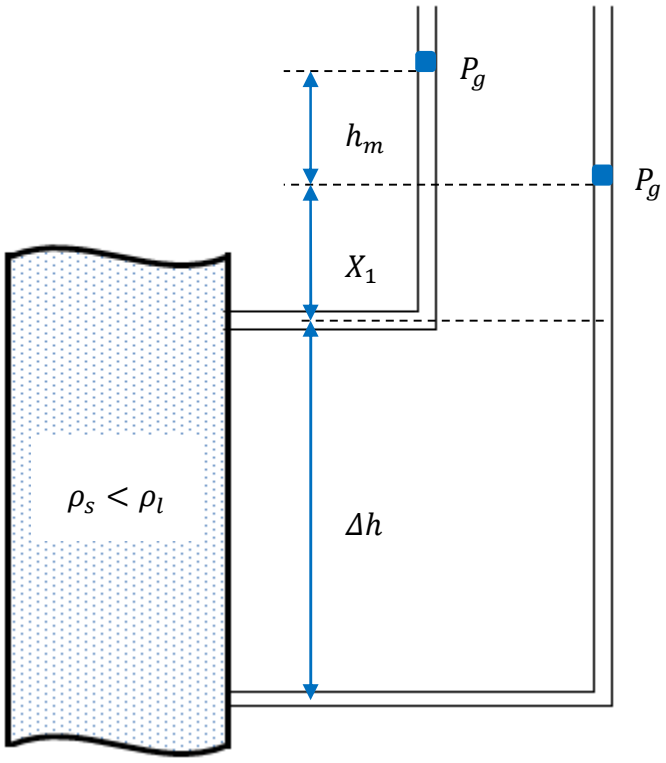

Figure 2-2: Schematic diagram for the measurement of the average solids holdup

Pressure drop across the bed

One of the common ways to find the minimum fluidization velocity is to measure the pressure drop across the bed.

$$\Delta P_{fbed} = \Delta P_{bed} - H_0 \rho_l g \tag{2.4}$$

Based on Equation (2.4), the frictional bed pressure drop depends on the total pressure drop across the bed and the pressure due to the height of the fluid. In the case of gas-solid fluidization, the second term is negligible because the density of the gas is small. On this basis, it is assumed that in gas-solid fluidization the frictional bed pressure drop is equal to the total pressure drop across the bed. However, in liquid-solid fluidization the second term is not negligible because the liquid density (in this study water) is high.

In order to find the pressure drop across the bed, one port was located close to the distributor. Another port was located at low enough height of the upcomer to ensure that the bed expansion of particles no longer reaches to this height. The pressure in points 1 and 3 is obtained by the following equations with manometers:

$$P_1 = X_1 \rho_l g + h_m \rho_l g + P_g \tag{2.5}$$

$$P_3 = X_1 \rho_l g + H_0 \rho_l g + X_2 \rho_l g + P_g \tag{2.6}$$

On the other hand, the pressure difference between points 1 and 3 inside the column is calculated by Equation (2.7):

$$P_3 - P_1 = \Delta P_{bed} + X_2 \rho_l g \tag{2.7}$$

By combination of Equations (2.5), (2.6) and (2.7), the total pressure drop across the bed is calculated by Equation (2.8):

$$\Delta P_{bed} = H_0 \rho_l g - h_m \rho_l g \tag{2.8}$$

Based on the definition of the frictional bed pressure drop in Equation (2.4), ΔP_{fbed} is obtained by Equation (2.9):

$$\Delta P_{fbed} = h_m \rho_l g \tag{2.9}$$

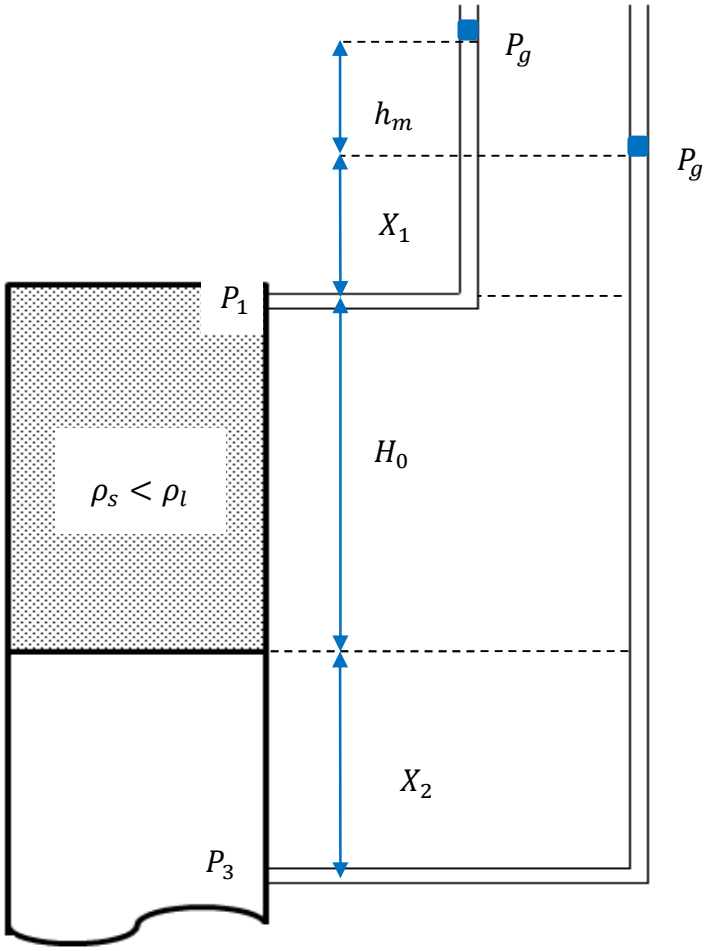

Figure 2-3: Schematic diagram for the measurement of the frictional bed pressure drop

Bed expansion

One way to measure the bed expansion during the fluidization is to observe the variation of the bed height versus the superficial liquid velocity visually. However, due to the fluctuation of particles at the bottom of the bed, this kind of measurement is not easy and accurate. Another way to measure the bed expansion is to measure it based on the variation of the pressure drop across the bed of particles.

Firstly, the average solids holdup at the section of the column occupied by both particles and water (Figure 2-4) is defined by the following equation:

$$\varepsilon_s = \frac{h_{m1}}{\Delta h_1} \times \frac{\rho_l}{\rho_l - \rho_s} \tag{2.10}$$

Since the fluidized bed is in the conventional fluidization regime and particles are dispersed homogeneously in both radial and axial directions, solids holdup is constant in the entire bed. In this case, the bed expansion is obtained by the following equation:

$$X = \frac{h_{m2}}{\varepsilon_s} \times \frac{\rho_l}{\rho_l - \rho_s} \tag{2.11}$$

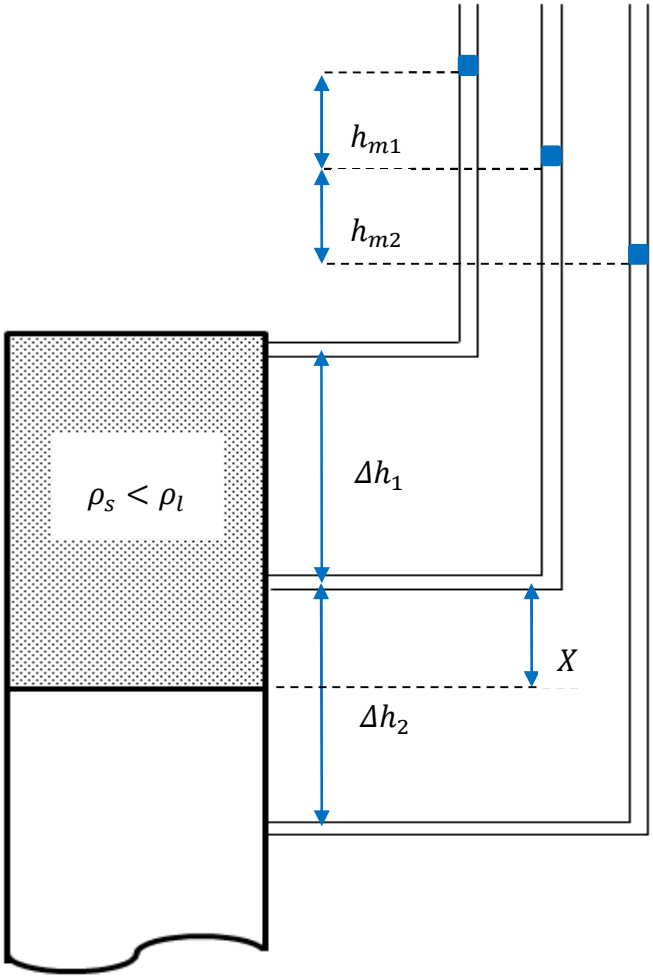

Figure 2-4: Schematic diagram for the measurement of the bed expansion

2.2.3 Optical fiber probe

In order to measure the local solids holdup, an optical fiber probe (OFP) containing a multitude of light transmitting fibers was used. The model of the probe was PV-5 manufactured by the Institute of Process Engineering, Chinese Academy of Sciences. The tip of the probe is circular with a diameter of 3.8 mm. This area includes approximately 8000 emitting and receiving quartz fibers. These fibers are arranged arbitrarily and the diameter of each fiber is 15 μm. In a simple expression, emitting fibers transfer the light from the source of the light to the measuring volume. Depending on the concentration of particles, the scattered light is reflected and conducted by the receiving fibers. The light is then diverted at the beam splitter and consequently transformed and amplified to the output voltage ranging from 0 to 5. Then, using an Analog/Digital converter the output voltage signal is fed to a personal computer.

The small size of the probe does not totally disturb the flow structure. This measuring device is not expensive and complicated. In addition, some problems such as temperature, humidity, electromagnetic fields and electrostatics do not influence the measurements [3].

The output of the optical fiber system is a voltage signal. It was calibrated precisely before each experiment. One of the best methods of calibration of the optical fiber probe was described by H. Zhang et al. [3]. Although in their study the optical fiber probe was used in a gas-solid fluidized bed, some procedures were also useful in a liquid-solid fluidized system. One of the procedures applied in this study was the use of two black boxes. One of the black boxes was full of particles and another one was empty. Before the main calibration, these two boxes were used to set the appropriate range for the zero and upper voltages.

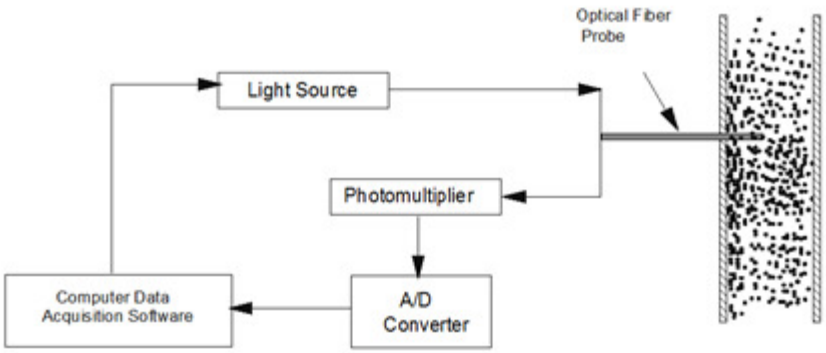

Figure 2-5: The optical fiber probe diagram for solids holdup measurement (Razzak et al. [4])

For each test, the calibration of the optical fiber probe was carried out on site. In this study, the calibration of the optical fiber probe was performed in the circulating fluidization regime. At the height of the downer in which the optical fiber probe measured the voltage, average solids holdup was measured by the two manometers as well. Thus, at different flowrates of liquid in the downer, several measurements were obtained by the optical fiber probe and the manometers. By using the relation between the solids holdup and electrical voltage, a linear relationship for the calibration of the optical fiber probe was obtained. During each experiment, the average solids holdup was measured by the manometers to ensure the accuracy of the optical fiber probe.

2.2.4 Electrical resistance tomography

Recently, a non-intrusive system of measurement named electrical resistance tomography (ERT) was introduced for the experimental research of multiphase flow. This system can measure the local phase distributions by electrical resistivity measurements of the multiphase flow. The system used in this study was manufactured by the En'Urga Inc. The ERT consists of sixteen conductivity sensors equally spaced around its wall, an electronic circuit and a PC-based data acquisition system. The inner diameter of ERT was built equal to the inner diameter of the downer to line up the sensors with the wall of the downer. ERT has the ability to acquire data at 250 frames per second. Based on the experiments performed in this report and by Razzak et al. [4], during each operating

frame, multiple driving currents are sequentially fed into a pair of neighboring electrodes. With the applied current source, electrical potential distributions are generated within the fluids and the wall. Electronic circuits sense voltages and currents between the electrodes and send them to a PC-based data acquisition system. Using the values of electrical potentials and currents, the local electrical conductivity of the liquid-solid mixture can be calculated and then reconstructed through a state-of-the-art optimization algorithm to provide the phase distributions. The conductivity distribution is converted into the solids holdup based on Maxwell's relation shown in Equation (2.12):

$$\varepsilon_s = \frac{2\sigma_l - 2\sigma_m}{2\sigma_l + \sigma_m} \tag{2.12}$$

where σ_l is the conductivity of continuous phase and σ_m is the conductivity of the mixture. The main concept behind the Maxwell`s equation is that the continuous phase of the mixture (in the present study water) should be electrically conductive and the second phase (Styrofoam bead) should include equal-sized spheres that are not electrically conductive [5].

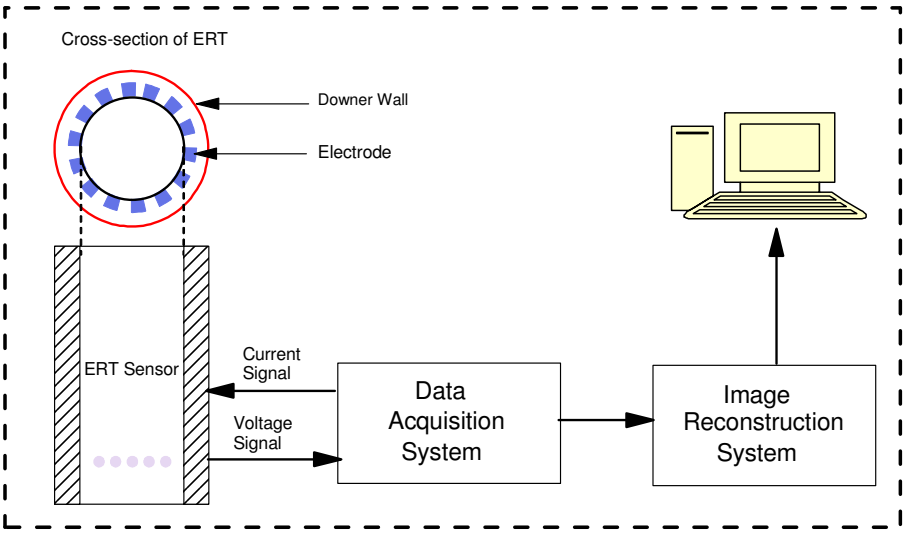

Figure 2-6: Schematic diagram of ERT (Razzak et al. [4])

Similarly to the calibration of the optical fiber probe, the ERT calibration was carried out on site for each experiment. The calibration of the ERT is important for obtaining

accurate data. In this work, M 541P compact precision conductivity meter was used to perform conductivity measurements quickly and reliably.

As shown in the structure of the inverse LSCFB, the system includes two water tanks connected to each other. Water is pumped from one tank and introduced to the downer and the upcomer. The second tank was designed to gather water from both columns. During the calibration of the ERT, the conductivity of water increased from 300 μ Si/cm to around 1400 μ Si/cm in seven or eight steps. In each step, 30 grams of table- salt was added to the first tank and water was circulated through the entire system (downer and upcomer). Then the conductivity of water in both tanks was measured. If the conductivity of water in both tanks was equal to each other, it was assumed that the conductivity of water in the entire system was the same. At this given conductivity, the ERT was run to take one second of data while only single phase liquid flowed through the test section. This collected data was treated and saved by a program made in $C++$.

This step was repeated to increase the conductivity of water to around 1400 μ Si/cm. During several experiments, it was found that if the number of steps was higher than six, the accuracy of the calibration and consequently results obtained by ERT in each test was high. At the final step of the calibration, data processing was done in the Matlab Environment and polynomial curve fitting was applied to obtain the calibration curve. The program showed an error regarding the best function which can fit the data. If the error was less than 1%, the accuracy of the results during the experiment was agreeable.

Nomenclature

A_r Cross sectional area of the upcomer (riser) (m^2)

A_d Cross sectional area of the downer (m^2)

H_o Solids inventory height (m)

h_m Height difference between the levels of water inside the manometers (m)

h_s Accumulated height of particles in measuring section (m)

P The pressure (Pa)

t Accumulation time of particles in the measuring section (s)

U_s Superficial solids velocity (m/s)

U_a Auxiliary liquid velocity (solids-free basis) – downer (m/s)

U_l Total liquid velocity (solids-free basis) – downer (m/s)

Greek Letters

ρ_l Density of the liquid (kg/m^3)

ρ_s Density of the solids (kg/m^3)

ε_s Solids holdup

Δh Distance between the pressure ports (m)

ΔP_{bed} The total bed pressure drop (Pa)

ΔP_{fbed} The frictional bed pressure drop (Pa)

σ_l The conductivity of the liquid $(\mu Si/cm)$

σ_m The conductivity of the mixture (liquid and particles) $(\mu Si/cm)$

References

[1] Long Sang (2013). "Particle Fluidization in Upward and Inverse Liquid-Solid Circulating Fluidized Bed". The University of Western Ontario, PhD Thesis.

[2] Zhu, J.-X., D. G. Karamanev, A. S. Bassi and Y. Zheng (2000). "(Gas-) liquid-solid circulating fluidized beds and their potential applications to bioreactor engineering". The Canadian Journal of Chemical Engineering 78(1): 82-94.

[3] Zhang, H., P. M. Johnston, J. X. Zhu, H. I. de Lasa and M. A. Bergougnou (1998). "A novel calibration procedure for a fiber optic solids concentration probe". Powder Technology 100(2-3): 260-272.

[4] Razzak, S. A., S. Barghi, J.-X. Zhu (2009). "Application of electrical resistance tomography on liquid–solid two-phase flow characterization in an LSCFB riser". Chemical Engineering Science 64(12): 2851-2858

[5] Mi, Y., M. Ishii, L.H. Tsoukalas (2001). "Flow regime identification methodology with neural networks and two-phase flow models". Nuclear Engineering and Design 204(1-3): 87–100

Chapter 3

3 The axial hydrodynamic behavior of light particles in an Inverse Liquid-Solid Circulating Fluidized Bed

3.1 Introduction

Inverse liquid-solid fluidization refers to a two-phase system where solid particles with density lower than liquid density are suspended by a stream of liquid flowing in the opposite direction to buoyancy. In the inverse liquid-solid fluidization, by increasing the stream of liquid and reaching the minimum fluidization velocity, particles move away from each other and the bed of the particles expands slowly in a downward direction from the boundary of the fix bed. This kind of fluidization regime is named conventional inverse fluidization where there is a clear boundary between the dense region of particles in the top and the bottom freeboard which is occupied by liquid [1].

The advantages and the applications of the inverse liquid-solid conventional fluidized reactors have been shown in last two decades. In the area of the biotechnology, Nikolov and Karamanev [2] found that a bioreactor working under these conditions would be able to control the biofilm thickness. Thus, the application of this bioreactor was described in different reports for such applications as anaerobic digestion of distillery effluent [3] and biological aerobic wastewater treatment [4, 5]. The previous reports on the hydrodynamics of inverse liquid-solid conventional fluidization showed that the hydrodynamics of inverse liquid-solid fluidization is different from that of an upward one. Fan et al. [6] used experimental bed expansion data to modify the Richardson and Zaki model in terms of Reynolds number, Archimedes number and liquid holdup. Karamanev and Nikolov [7] found that the Richardson and Zaki model predicted their experimental data for particles of different characteristics agreeably when the terminal velocity was calculated by the model of free rising particles proposed by them [8]. Ulaganathan and Krishnaiah [9] studied a semi-fluidized regime before complete fluidization. They proposed empirical correlations for the bed expansion in the semi-fluidized and fully fluidized bed regime in terms of Reynolds number, Archimedes

numbers, and liquid-solid density difference. Renganathan and Krishnaiah [10] studied the voidage fluctuations, axial voidage profile and bed expansion. They proposed an explicit correlation for the terminal velocity of a free rising particle.

When particles with density lower than the density of the liquid are fluidized in a column known as a downer, particles begin to be transported out of the bed after reaching the liquid velocity of the critical transient point [1]. Under this condition, particles are carried out of the column by the downward liquid. If particles are separated at the bottom of the downer and stored in another column, particle recirculation can be achieved between two columns by continuously feeding the particles to the top of the downer. Under these conditions, the boundary between the two phases is not clear in the downer and particles are dispersed in the entire column. Generally for the upward liquid-solid fluidization, it was shown that liquid-solid fluidized bed reactors working in the circulating fluidizing regime have certain advantages compared to the reactors working under the conventional fluidizing regime. Therefore, liquid-solid circulating fluidized bed reactors have been used in different areas of chemical engineering. In the field of waste water treatment, excellent lab-scale results led to the establishment of a pilot scale liquid-solid circulating fluidized bed for the municipal wastewater treatment [11]. In the area of continuous ion exchange processes, the application of liquid-solid circulating fluidized bed has resulted in successful continuous protein recovery [12]. Regarding the biochemical production, Patel et al. [13] introduced a novel liquid-solid circulating fluidized bed bioreactor for the fermentative production of lactic acid. In the bio-refining processes, Trivedi et al. [14] used a liquid-solid circulating fluidized bed as a continuous reactor for polymerization of phenol.

The study of the hydrodynamic behavior of LSCFB reactors is important for determining the capabilities of these reactors. In contrast to the inverse LSCFB, the hydrodynamic behavior of upward liquid-solid circulating fluidized beds have been well documented. The axial hydrodynamics of the liquid-solid circulating fluidized bed including the variation of the axial phase distribution with varying solids circulation rate was studied by Zheng et al. [15]. In that study, the effects of different factors such as solids inventory in the downcomer were reported as well. In addition, a comprehensive study on the

stability of liquid-solid circulating fluidized bed was reported in a study by Zheng and Zhu [16]. The demarcation of conventional fluidization regime from the circulating fluidization regime and empirical relation to measure the critical velocity when circulation of particles begins are important in the hydrodynamic study. Liang et al. [17] proposed a regime map for the operation of the liquid-solid upward fluidization including the conventional fluidization, circulating fluidization and transport regimes. In comparison with the relation offered by Liang et al. [17], Zheng and Zhu [18] proposed an onset velocity correlation for liquid-solid circulating fluidized bed ignoring the effects of geometry of the system.

Recently, by combining the concepts of inverse liquid-solid fluidization and of circulating fluidization, a novel type of two-phase system, "Inverse Liquid-Solid Circulating Fluidized Bed", was proposed by Sang [19]. The aim of the current work is to study the hydrodynamic behavior of this novel two-phase system containing particles with density lower than the liquid density. Firstly, some experiments were conducted to compare the results from the present two-phase system with the previous results which had been obtained for the upward LSCFB. Then the solids inventory in the upcomer was increased to observe its effect on the solids circulation rate and the average solids holdup in the downer under the new conditions. Finally, a liquid stream was introduced from the top of the upcomer to study its effect on the downer hydrodynamics where solids circulation rate and average solids holdup were measured and compared with results in which flowrate of the liquid in the upcomer was zero.

3.2 Materials and Methods

A schematic diagram of the inverse liquid-solid circulating fluidized bed (ILSCFB) reactor used in this study is shown in Figure 3-1. The main parts and the operation of this system were discussed in chapter 2.

The solids circulation rate and the superficial liquid velocity were measured by solids circulation measuring device. This device was located at the bottom of the upcomer. Six ports at different heights were placed along the downer and connected to the six

manometers. By measuring the pressure drop, the average solids holdup is obtained in the downer.

The solid phase was represented by spherical Styrofoam beads with a mean diameter of 0.8 mm and a density of 28 kg/m^3 while the liquid phase was tap water. All experiments were performed at ambient temperature.

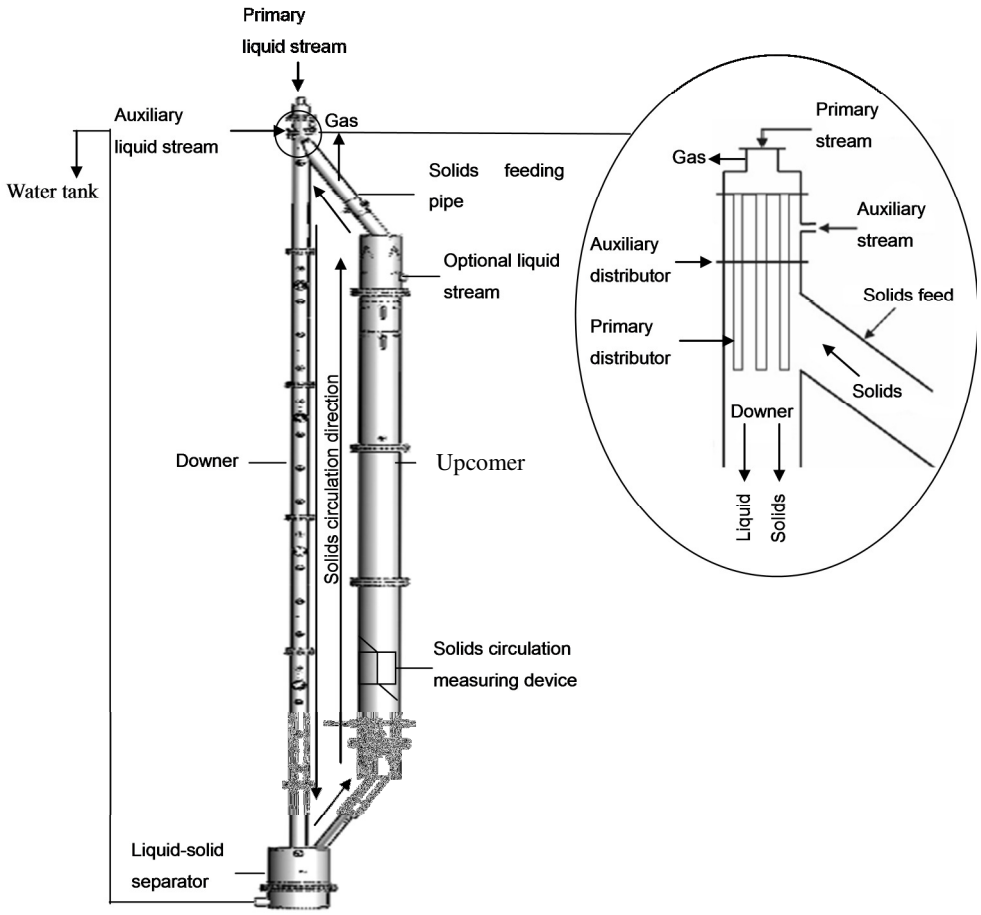

Figure 3-1: Schematic diagram of the inverse LSCFB reactor designed by Sang [19]

3.3 Results and Discussion

Circulating fluidization regime in the downer is obtained when the total liquid velocity in this column is higher than the terminal rising velocity of particles. Continuous feeding of particles at the top of the downer significantly depends on the auxiliary flowrate. Liquid

stream introduced into the downer from the auxiliary distributor mobilizes the particles transported from the solids feed pipe to the downer and accumulated between the main and auxiliary distributor. Thus, once the particles reach the front of the main distributor, they are carried by the main liquid stream in downward direction. If the auxiliary flowrate is set at zero, the particles stay in the area between the auxiliary distributor and main distributor, hence the circulation of particles is no longer occurring.

Through the solids feed pipe, the particles are transported to the top of the downer slowly in a packed state. A minor portion of the auxiliary liquid stream flowing into the solids feed pipe helps to reduce the friction between the particles and the wall.

The first set of the experiments was performed under the condition where the total solids inventory in the upcomer was 0.9 meters (when all the particles are stored in the upcomer). Figure 3-2-A shows the variation of the superficial solids velocity versus the superficial liquid velocity at four different auxiliary liquid velocities. It is obvious that at a fixed auxiliary liquid velocity, superficial solids velocity increased in the downer with increasing the total liquid velocity. In addition, higher auxiliary flowrate resulted in higher superficial solids velocity at a given total liquid velocity.

Similarly to the results reported by Zheng et al. [15] for the upward LSCFB, two distinct zones during the circulating fluidization regimes were observed for the inverse LSCFB. After the onset of the circulation, by increasing the superficial liquid velocity, the superficial solids velocity increased sharply. This zone was referred to the initial circulating fluidization zone [1]. However, after reaching a certain point, the superficial liquid velocity did not increase significantly as the superficial solids velocity increased further. In this case, the transition from the initial circulating fluidization zone to the developed circulating fluidized zone was obtained.

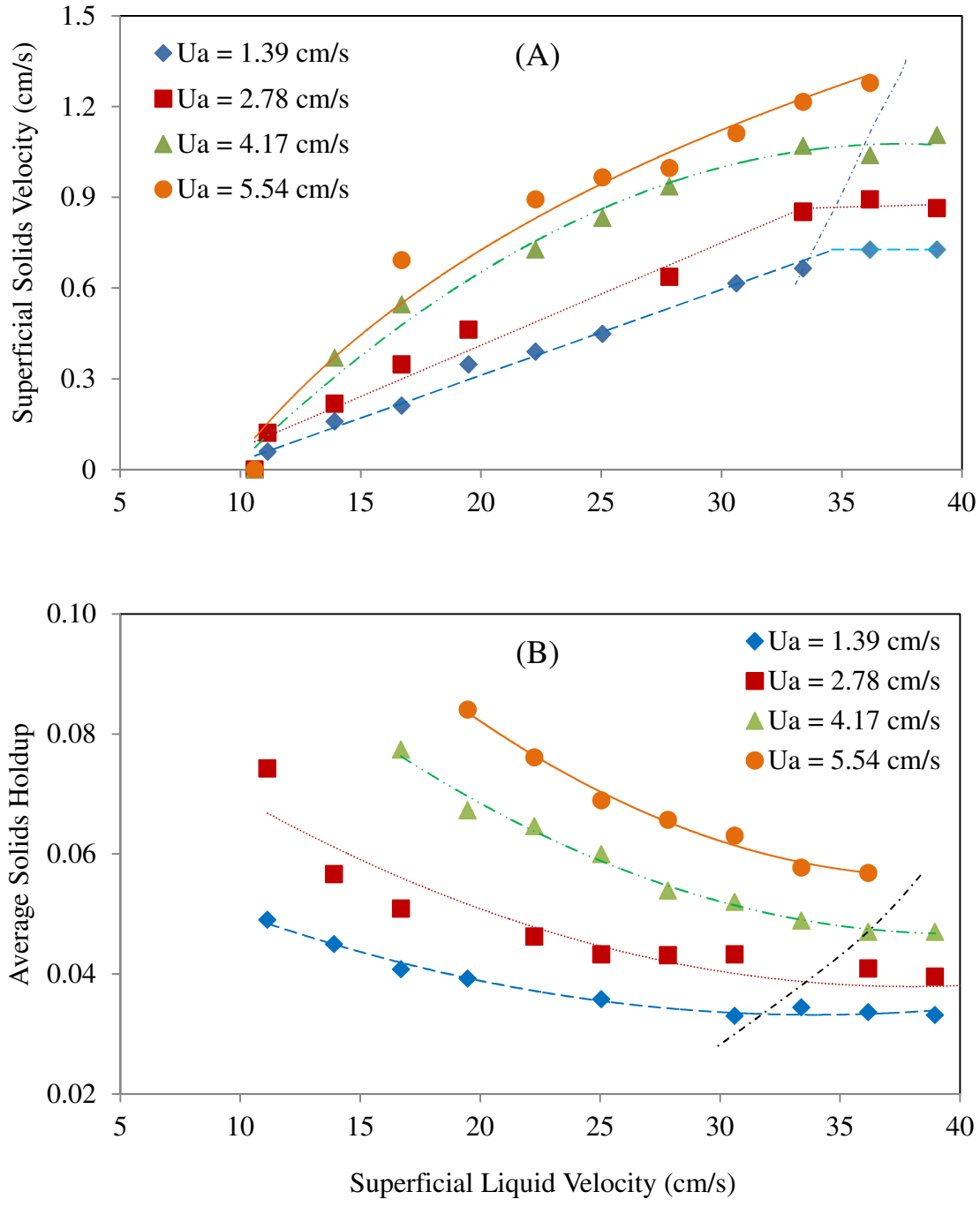

Figure 3-2: Variation of (A) the superficial solids velocity and (B) the average solids holdup versus the superficial liquid velocity at different auxiliary liquid velocities in the downer

At low auxiliary flowrates, the existence of the developed circulating fluidized zone was observed when the solids circulation rate increased insignificantly with the increase of the total liquid velocity. However, at high auxiliary liquid velocities, the increase of superficial solids velocity with increasing the superficial liquid velocity continued considerably even at high liquid velocities and the developed circulating fluidized zone was not obtained in the downer. In the previous study by Zheng et al. [15] for the upward LSCFB, it was proposed that at high auxiliary flowrates, the stable operating range decreased in comparison to lower auxiliary flowrates. Similar behavior was also observed in the inverse liquid-solid circulating fluidized bed as well. For instance, at auxiliary liquid velocity of $U_a = 2.78\ cm/s$, the circulation of particles started at lower superficial liquid velocity without facing the risk of unstable operation and the system was operated in higher superficial liquid velocities as well. In contrast, at auxiliary liquid velocity of $U_a = 5.54\ cm/s$, the circulation of the particles commenced at total liquid velocity of $U_l = 16.7\ cm/s$ and before that the system faced an unstable operation and no circulation of the particles was achieved in the system. In addition, it was observed that the developed fluidization zone was not obtained at high superficial liquid velocities and the further increasing of the superficial liquid velocity was not possible because of the pump capacity limitation.

Figure 3-2-B shows the variation of the average solids holdup versus the superficial liquid velocity at four auxiliary liquid velocities in the downer. Based on Figure 3-2, at different auxiliary liquid velocities, higher auxiliary flowrate led to feeding more particles and thus to higher average solids holdup in the downer.

At a fixed auxiliary flowrate, the average solids holdup in the downer decreased as the superficial liquid velocity was increased. This trend is completely similar to the previous results for the riser of the upward LSCFB. In previous results reported by Zheng et al. [15] and Liang et al. [17], it was concluded that increasing the superficial liquid velocity can result in increasing the particles velocity and decreasing the residence time of the particles in the riser which was observed in the current results for the downer of the inverse LSCFB.

Two different zones including the initial circulating fluidization and developed circulating fluidized zones are evident from Figure 3-2-B. At the beginning of the circulation, the average solids holdup in the downer decreased quickly. After reaching a certain velocity by further increasing the superficial liquid velocity, the average solids holdup decreased slowly in the downer. This can be explained based on Figure 3-2-A where the variation of the superficial solids velocities at higher superficial liquid velocities was insignificant and the regime of the two-phase flow in the downer was at the developed circulating fluidized zone.

Looking at Figure 3-3, it is clear that at higher superficial solids velocities, due to feeding more particles into the downer, higher average solids holdup was obtained at a total liquid velocity in the downer. In addition, at a fixed superficial solids velocity, the increase in the superficial liquid velocity led to the decrease of the average solids holdup. Such decrease was more evident at lower superficial liquid velocities, but with further increasing the superficial liquid velocity, the average solids holdup in the downer decreased slowly.

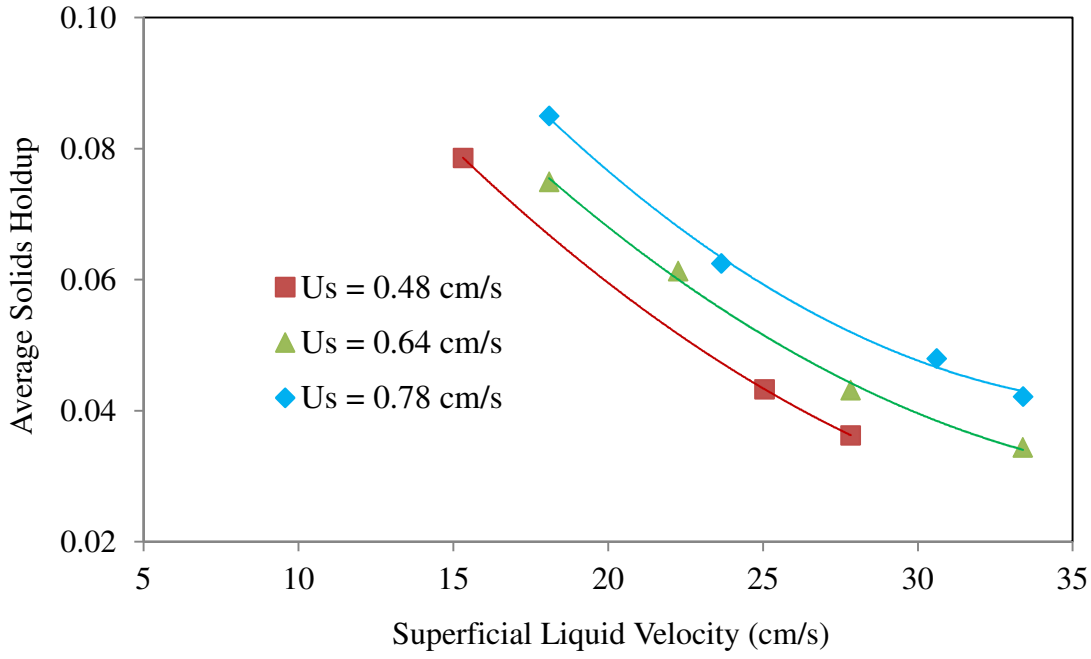

Figure 3-3: Variation of the average solids holdup versus the superficial liquid velocity at different superficial solids velocities in the downer

One hydrodynamic advantage of the inverse LSCFB is related to the uniform distribution of particles in the axial direction. The variation of the axial solids holdup under the circulating fluidization regime is shown in Figure 3-4. In order to observe the axial solids holdup in the downer at two different zones marked in Figure 3-2, two different liquid velocities were chosen. When the superficial liquid velocity was high in the downer ($U_l = 33.39\ cm/s$) and the regime of circulating fluidization was in the developed circulating fluidized zone, uniform axial average solids holdup was observed in the downer. In addition, even when the superficial liquid velocity was low ($U_l = 16.7\ cm/s$) in the downer and the regime of the circulating fluidization was still in the initial circulating fluidization zone, axial solids holdup was observed to be uniform.

In the previous study of the upflow LSCFB by Zheng et al. [15] for lighter particles such as plastic ($\rho_s = 1100\ kg/m^3$) and glass ($\rho_s = 2490\frac{kg}{m^3}$) beads, uniform distribution of the particles was observed in both zones. When heavier particles (steel shots with $\rho_s = 7000\ kg/m^3$) were used, the axial solids holdup was non-uniform in the initial circulating fluidization zone, but uniform at developed circulating fluidized zone [15]. It is reasonable to assume that the density difference influences the distribution of particles in the axial direction. When the density difference was large ($\rho_s - \rho_l = 6000\frac{kg}{m^3}$ for steel shots) the non-uniformity of particles distribution was observed, but at low density differences ($\rho_s - \rho_l = 100\frac{kg}{m^3}$ for plastic beads and $\rho_s - \rho_l = 1490\frac{kg}{m^3}$ for glass beads) a uniform distribution of the particles was found in the upward LSCFB. On this basis, it can be expected that since the density difference cannot exceed above $1000\frac{kg}{m^3}$ in the case of the inverse LSCFB having water as a liquid phase, the particles distribution is always uniform in the axial direction. However, particles with different densities should be used in the future experiments to prove this assumption.

As it was discussed in Figures 3-2 and 3-3 and it is obvious from Figure 3-4, at a constant superficial liquid velocity, higher superficial solids velocity resulted in higher average solids holdup in the downer.

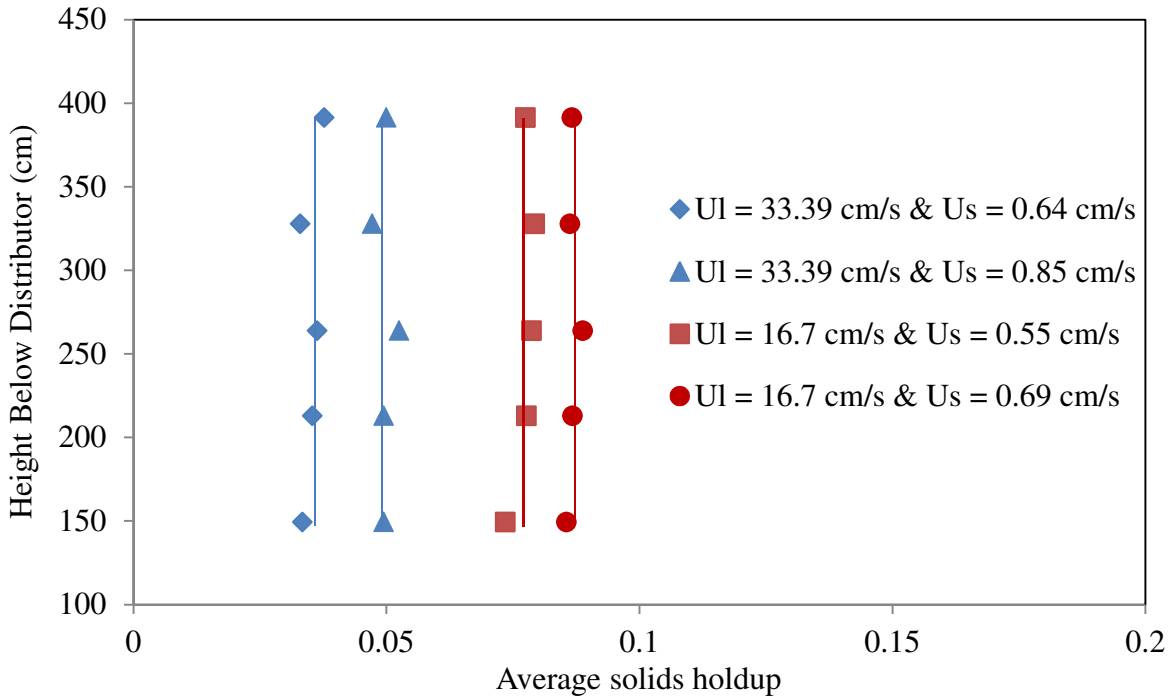

Figure 3-4: Variation of the axial solids holdup distribution under the circulating fluidization regime

Figure 3-5 shows the variation of the superficial solids velocity and the average solids holdup versus the superficial liquid velocity at a constant auxiliary flowrate, but with two different solids inventories. It was expected based on the previous results obtained for the upflow LSCFB that increasing the solids inventory would result in increasing the solids circulation rate [16]. We found out that, when solids inventory increased, the pressure drop increased across the bed of particles in the upcomer. Thus, a higher pressure head at the top of the upcomer provided higher feeding rate of particles into the downer. Consequently, higher solids holdup was observed in the downer.

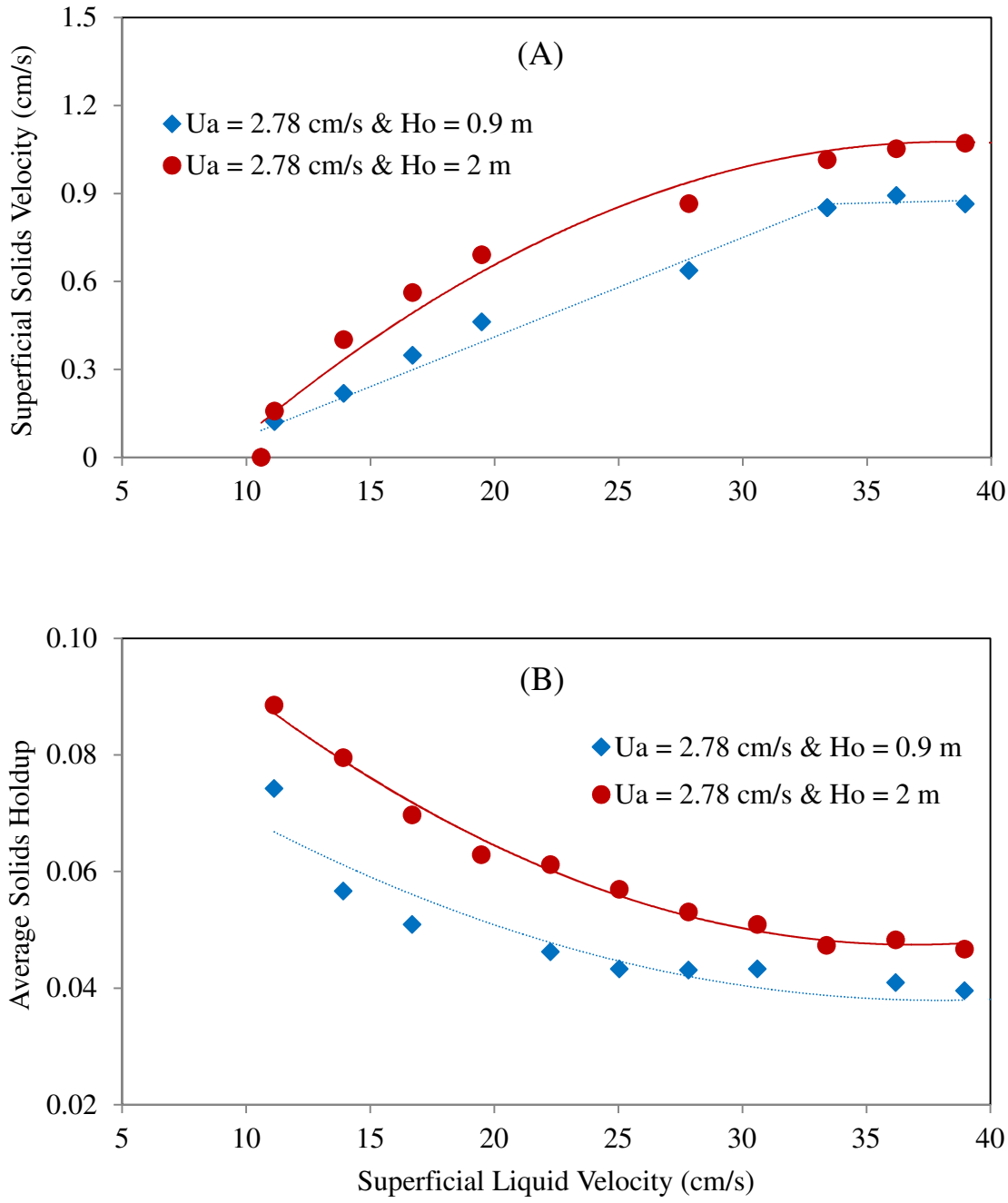

Figure 3-5: Effect of solids inventory in the upcomer on (A) the superficial solids velocity and (B) the average solids holdup in the downer at auxiliary liquid velocity of $U_a = 2.78\ cm/s$

Figure 3-6-A shows the effect of the counter current flow in the upcomer on the variation of the superficial solids velocity versus the superficial liquid velocity in the downer at a

constant solids inventory. Once a certain stream of water was introduced from the top of the upcomer, a counter current flow was formed in it. The stream of water introduced from the top of the upcomer flowed in the downward direction while particles entered from the separator to the upcomer moved in the upward direction.

Based on Figure 3-6-A, at auxiliary liquid velocity of U_a = 2.78 cm/s, when the flowrate of water in the upcomer was higher than zero, superficial solids velocity in the downer considerably increased compared to the case when the flowrate of water in the upcomer was zero. When a certain stream of liquid was entered from the top of the upcomer, solids inventory stored at its top were mobilized. Under this condition, the friction between the particles decreased and particles could move to the solids feed pipe much easier. Therefore, because of more particles feeding into the downer, higher average solids holdup was achieved in the downer.

For the future applications of the inverse LSCFB in different areas, it is necessary that the upcomer is operated under the counter current flow while downer is operated at circulating fluidization regime. Experimentally, it was found in Figure 3-6 that at a fixed total liquid velocity, the liquid flow introduced from the top of the upcomer increased the superficial solids velocity and average solids holdup in the downer in comparison to zero flow. Interestingly, another important feature of the counter current flow in the upcomer found in this study was that the continuous circulation of the particles in the entire system could be controlled at low auxiliary liquid velocity.

Figure 3-7 shows the combination of the main and auxiliary velocities to reach the constant superficial solids velocity of $U_s = 1.4\ \mathrm{cm/s}$ in the downer under two conditions ($U_r = 0\ \mathrm{cm/s}$ and $U_r = 0.4\ \mathrm{cm/s}$). For example, at the total superficial liquid velocity of $U_l = 32.84\ \mathrm{cm/s}$ in the downer, when no liquid stream introduced from the top of the upcomer, the auxiliary liquid velocity of $U_a = 5\ cm/s$ was set to reach the superficial solids velocity of $U_s = 1.4\ cm/s$. On the other hand, when a certain liquid flowrate was obtained in the upcomer, the auxiliary liquid velocity of $U_a = 0.93\ cm/s$ was fixed to reach the superficial solids velocity of $U_s = 1.4\ cm/s$.

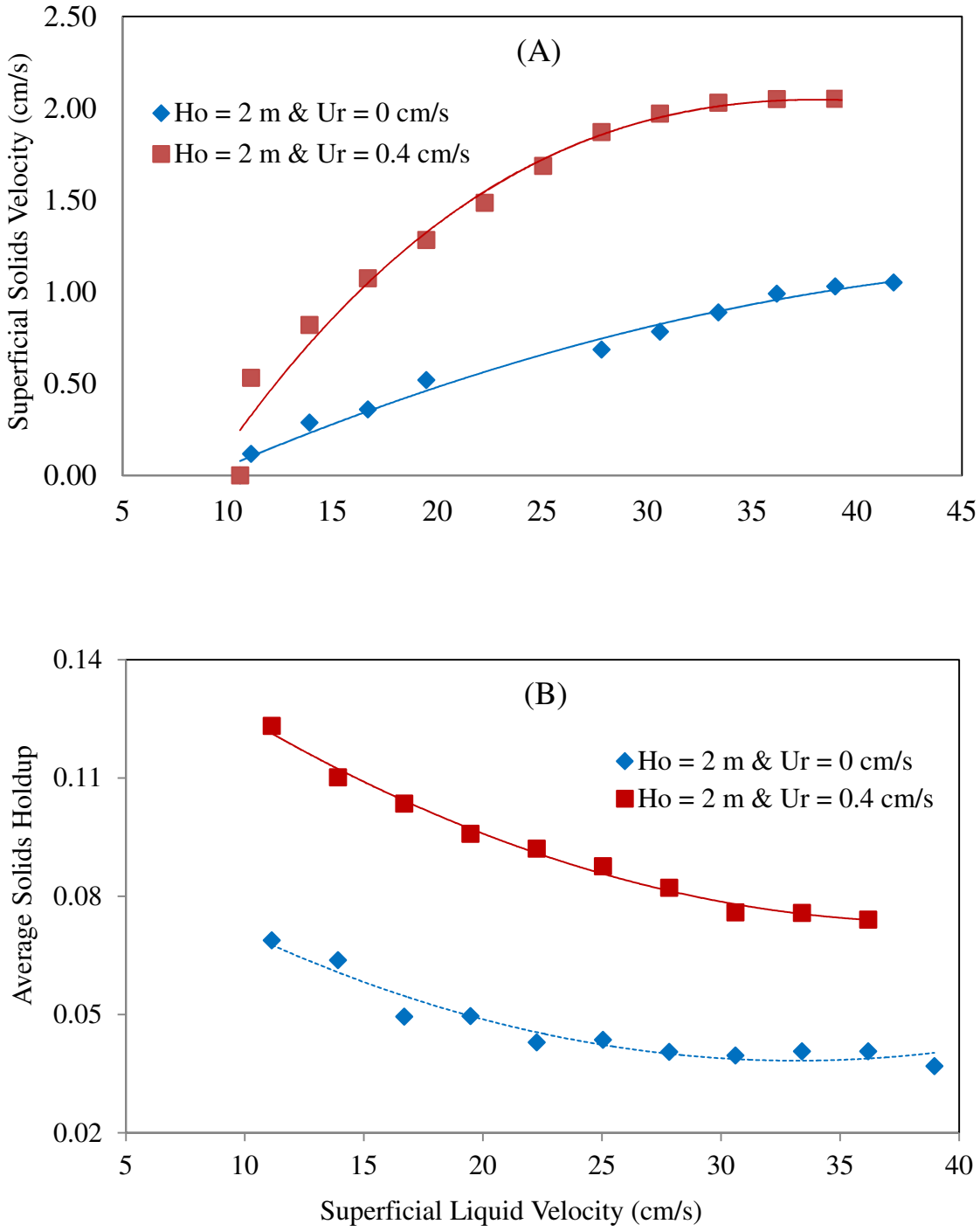

Figure 3-6: Effect of counter current flow in the upcomer on (A) the superficial solids velocity and (B) the average solids holdup at auxiliary liquid velocity of $U_a = 1.39$ cm/s

The importance of the operation of the system at lower auxiliary liquid velocity is related to the stable operation of the system discussed in Figure 3-2 and was reported for the upward LSCFB by Zheng et al. [15]. It was observed in this study that high auxiliary liquid velocities should be obtained to have higher solids circulation rate and consequently higher dispersion of the particle holdup in the downer. On the other hand, in both the results reported by Zheng et al. [15] for the upward LSCFB and in this study, the operation of the system at high auxiliary liquid velocities had limited range because the operation of the system become unstable and circulation of particles no longer occurred. On this basis, the counter current flow in the upcomer provided not only the condition with higher solids circulation rate and particles distribution in the downer but the system was also operated at low auxiliary liquid velocities to reduce the risk of unstable operation.

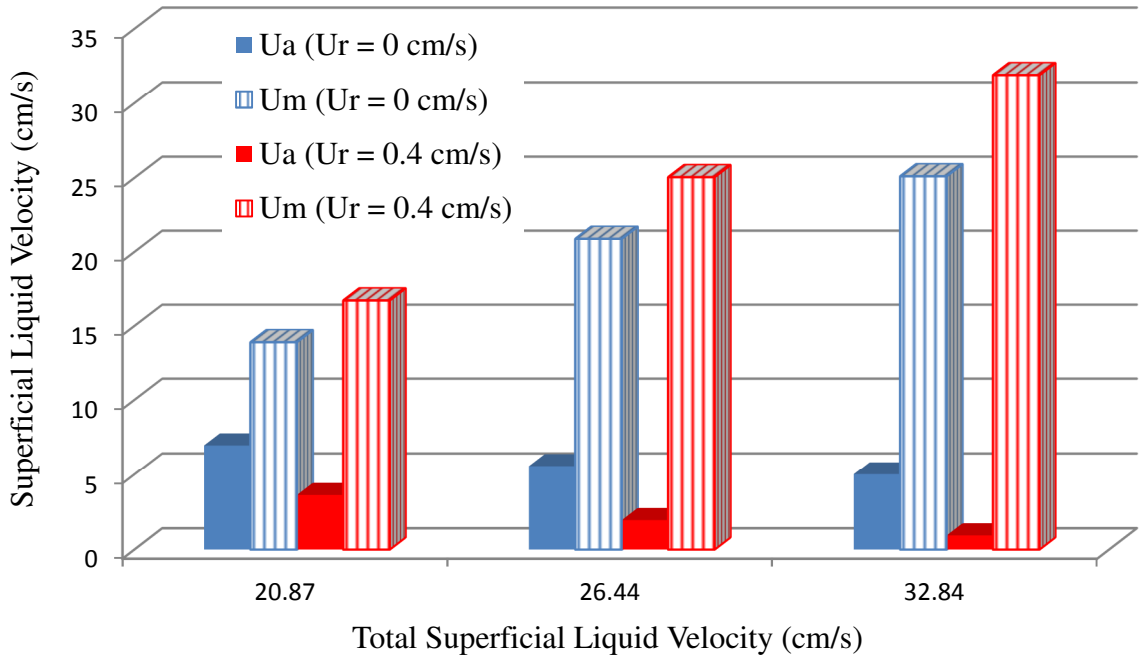

Figure 3-7: Comparison of ratios of the main and auxiliary liquid velocities under two different conditions ($U_r = 0\ cm/s$ and $U_r = 0.4\ cm/s$) at superficial solids velocity of $U_s = 1.4\ cm/s$

3.4 Conclusion

The axial hydrodynamics of a novel reactor, "Inverse Liquid-Solid Circulating Fluidized Bed", was studied under a wide range of operating conditions. These results can be useful for finding the operational boundaries and the optimal conditions for different process applications. The variation of the superficial solids velocity and the average solids holdup in the downer as a function of the superficial liquid velocity showed the existence of two different zones in the circulating fluidization regime, initial and fully developed ones. Similar two zones were reported for the upward LSCFB as well. In both zones, the axial distribution of particle holdup in the downer was uniform. The effects of the solids inventory and counter current flow in the upcomer on solids circulation rate and average solids holdup in the downer was studied. It was shown that under counter current flow in the upcomer, higher solids circulation rate and average solids holdup were obtained in the downer with lower risk of unstable operation.

Nomenclature

H_o Solids inventory height (m)

U_s Superficial solids velocity (m/s)

U_m Main liquid velocity (solids-free basis) – downer (m/s)

U_a Auxiliary liquid velocity (solids-free basis) – downer (m/s)

U_l Total liquid velocity (solids-free basis) – downer (m/s)

U_r Total liquid velocity (solids-free basis) – upcomer (riser) (m/s)

Greek Letters

ρ_l Density of the liquid (kg/m^3)

ρ_s Density of the solids kg/m^3)

ε_s Solids holdup

References

[1] Zhu, J.-X., D. G. Karamanev, A. S. Bassi and Y. Zheng (2000). "(Gas-) liquid-solid circulating fluidized beds and their potential applications to bioreactor engineering". The Canadian Journal of Chemical Engineering 78(1): 82-94.

[2] Nikolov, L. and D. Karamanev (1987). "Experimental Study of the Inverse Fluidized Bed Biofilm Reactor". Canadian Journal of Chemical Engineering 65(2): 214-217.

[3] Sowmeyan, R. and G. Swaminathan (2008). "Performance of inverse anaerobic fluidized bed reactor for treating high strength organic wastewater during start-up phase". Bioresource Technology 99(14): 6280-6284.

[4] Nikolov, L., D. Karamanev, T. Penev, and D. Dimitrov (1990). "Full-Scale Inverse Fluidized Bed Biofilm Reactor for Wastewater Treatment" 2nd Int. Biotechnol. Conf.: Asian-Pacific Biotechnol. Conf., 112, Seoul, Korea.

[5] Karamanev, D. G. and L. N. Nikolov (1996). "Application of inverse fluidization in wastewater treatment: From laboratory to full-scale bioreactor". Environmental Progress 15(3): 194-196.

[6] Fan, L.-S., K. Muroyama and S. H. Chern (1982). "Hydrodynamic Characteristics of Inverse Fluidization in Liquid-Solid and Gas-Liquid-Solid Systems". The Chemical Engineering Journal 24(2): 143-150.

[7] Karamanev, D. G. and L. N. Nikolov (1992b). "Bed expansion of liquid–solid inverse fluidization". AICHE Journal 38(12): 1916–1922

[8] Karamanev, D. G. and L. N. Nikolov (1992a). "Free rising spheres do not obey Newton's law for free settling". AICHE Journal 38(11): 1843–1846.

[9] Ulaganathan, N. and K. Krishnaiah (1996). "Hydrodynamic characteristics of two-phase inverse fluidized bed". Bioprocess and Biosystems Engineering 15(3): 159-164.

[10] Renganathan, T. and K. Krishnaiah, (2005). "Voidage characteristics and prediction of bed expansion in liquid–solid inverse fluidized bed". Chemical Engineering Science 60(10): 2545–2555.

[11] Chowdhury, N., J. Zhu, G. Nakhla, A. Patel and M. Islam (2009). "A novel liquid-solid circulating fluidized-bed bioreactor for biological nutrient removal from municipal wastewater". Chemical Engineering and Technology 32(3): 364-372.

[12] Lan, Q., J. X. Zhu, A. S. Bassi, A. Margaritis, Y. Zheng and G. E. Rowe (2001). "Continuous protein recovery using a liquid-solid circulating fluidized bed ion exchange system: Modelling and experimental studies". Canadian Journal of Chemical Engineering 79(4): 687-687.

[13] Patel, M., A. S. Bassi, J. J. X. Zhu and H. Gomaa (2008). "Investigation of a dual-particle liquid-solid circulating fluidized bed bioreactor for extractive fermentation of lactic acid". Biotechnology Progress 24(4): 821-831.

[14] Trivedi, U., A. Bassi, J. Zhu (2006). "Continuous enzymatic polymerizationof phenol in a liquid-solid circulating fluidized bed". Powder Technology 169(2): 61–70.

[15] Zheng, Y., J.-X. Zhu, J. Wen, S. A. Martin, A. S. Bassi and A. Margaritis (1999). "The axial hydrodynamic behavior in a liquid-solid circulating fluidized bed". Canadian Journal of Chemical Engineering 51(50): 16242-16250

[16] Zheng, Y. and Jesse Zhu (2000). "Overall pressure balance and system stability in a liquid–solid circulating fluidized bed". Chemical Engineering Journal 79(2): 145–153.

[17] Liang, W., S. Zhang, J.-X. Zhu, Y. Jin, Z. Yu and Z. Wang (1997). "Flow characteristics of the liquid-solid circulating fluidized bed". Powder Technology 90(2): 95-102.

[18] Zheng, Y. and J.-X. Zhu (2001). "The onset velocity of a liquid-solid circulating fluidized bed". Powder Technology 114(1-3): 244-251.

[19] Long Sang (2013). "Particle Fluidization in Upward and Inverse Liquid-Solid Circulating Fluidized Bed". The University of Western Ontario, PhD Thesis.

Chapter 4

4 Radial distribution of light particles in an Inverse Liquid-Solid Circulating Fluidized Bed

4.1 Introduction

Liquid-solid circulating fluidized beds have been a subject of interest not only in research investigations but also in different areas of chemical engineering processes in the recent years. Several advantages of LSCFB reactor such as effective contact between particles and liquid, good mixing and controlling the phase holdup via solids circulation rate in the whole reactor have been reported [1]. Various applications of LSCFB reactors for instance in waste water treatment [2], continuous protein recovery [3], fermentative production of lactic acid [4] and polymerization of phenol [5] have demonstrated the capability of LSCFB reactor in the ongoing studies.

In this work, the solid particles having density higher than that of the continuous liquid, will be named “heavy particles”, while particles with density lower than that of the surrounding liquid will be referred to as “light particles”. As already established in the literature, a fluidized bed containing light particles, fluidized by a downflowing liquid, is named “inverse fluidized bed”. Different applications of inverse liquid-solid fluidization technique in biotechnology have been proposed and inverse liquid-solid fluidized bed bioreactor has been used for anaerobic digestion of distillery effluent [6], bioleaching of metals [7], antibiotic production [8] and biological aerobic wastewater treatment [9, 10].

Almost all of the previous reports on the inverse liquid-solid fluidization were limited to the conventional fluidization regime. The most important studies such as modification of Richardson and Zaki equation for inverse liquid-solid fluidization [11], bed expansion characteristics and minimum fluidization velocity [12], dynamics of the free rise of a light solid sphere in liquid [13], and small inertia of particles and their effects on mass transfer [14] have shown that the hydrodynamics of the conventional inverse liquid-solid

fluidized bed is different with that of the upward one. Recently, advantages of the inverse liquid-solid fluidization and the concept of circulating fluidization were combined and the novel type of the reactor, "Inverse Liquid-Solid Circulating Fluidized Bed" was proposed by Sang [15].

It should be noted that due to the opposite directions of the settling of light and heavy solid particles (upwards and downwards, respectively); the riser of the LSCFB corresponds to the downer of the ILSCFB. In general, the entire ILSCFB is an upside-down version of the LSCFB. It is expected that the light-particle inverse liquid-solid circulating fluidized bed would have a different behavior as compared to the heavy-particle liquid-solid circulating fluidized bed. This expectation is based on the fundamental difference between the behavior of a single light and single heavy particle in liquid, and especially the difference in the particle-turbulence interactions.

The study of the radial flow structure of a fluidized bed is important because of its effects on the mass transfer and reactions taking place on the liquid-solid interface in both inverse and upward liquid-solid circulating fluidized bed reactors [16]. In the case of liquid-solid circulating fluidized bed in which the solids phase was represented by particles with density higher than liquid density, different methods of measurement such as manometer, pressure transducer, electrical conductivity probes, optical fiber probes and different kinds of image processing have been used to measure the phase distribution. Liang et al. [16] used electrical conductivity probes to measure the phase distribution in the riser of LSCFB. In their study, non-uniformity of solids holdup in radial direction was reported. Zheng et al. [17] used an optical fiber probe to measure the radial particles distribution in the riser of LSCFB. They reported that solids holdup is lower in the center of the column, but higher near the wall. In their study, particles with different densities were used to show how the radial distribution of particles was changed as a function of the particle density. Razzak et al. [18] used an image processing technique known as Electrical Resistance Tomography (ERT) in the riser of LSCFB to measure the phase holdup. They found an excellent agreement between the results of the ERT and of the optical fiber probe for the radial distribution of particles. In the study of radial flow

structure of gas-liquid-solid fluidized bed, Razzak et al. [19] also used the ERT to measure the local and average phase distribution.

So far, no one has studied the radial particle distribution in the inverse LSCFB. Taking into account the fundamental difference between the behavior of the light and heavy particles, it is expected that the hydrodynamics of the ILSCFB should be different from the LSCFB. In this work, the radial phase distribution of solid-liquid downflow in the downer of the inverse liquid-solid circulating fluidized bed reactor was studied. Three different measurement techniques including the manometers, an optical fiber probe and the ERT were employed to determine the solids holdup in the downer. Finally, results obtained from the inverse liquid-solid circulating fluidized bed reactor were compared to the upward LSCFB containing the particles with density higher than the water density.

4.2 Material and Methods

The set-up of inverse liquid-solid circulating fluidized bed (ILSCFB) system used in this study is shown in Figure 4-1. The main parts and the operation of this system were discussed in chapter 2.

In order to measure the solids circulation rate, a solids flowrate measurement device was located near the bottom of the upcomer. Six ports at different heights were placed along the downer and connected to six manometers. By measuring the pressure drop, the average solids holdup is obtained in the downer.

The probe model PV-5 was used to measure the local solids holdup. All the measurements by the optical fiber probe (OFP) were obtained from two different heights of 2.1 and 3.4 meters below the distributor to allow the formation of fully developed flow in the measurement sections. In addition, the measurement sections of the column for OFP were wrapped by black plastic to avoid the distorting effect of the external light.

In addition, ERT at the height of the 4.4 meters below the distributer was used to determine the local phase distribution via the electrical resistivity measurements of the liquid. Similarly to the measurements performed by Razzak et al. [18], radial

distributions were measured in seven radial positions from center to the wall at $\frac{r}{R} = 0$, 0.2034, 0.492, 0.6396, 0.7615, 0.8614, and 0.9518. The cross-sectional area of the ILSCFB downer was divided into six equal zones and all afore mentioned radial positions were taken at the central position of each equal zone.

The solid phase was spherical Styrofoam beads with a mean diameter of 0.8 mm and a density of 28 kg/m^3 while the liquid phase was tap water. All experiments were performed at ambient temperature.

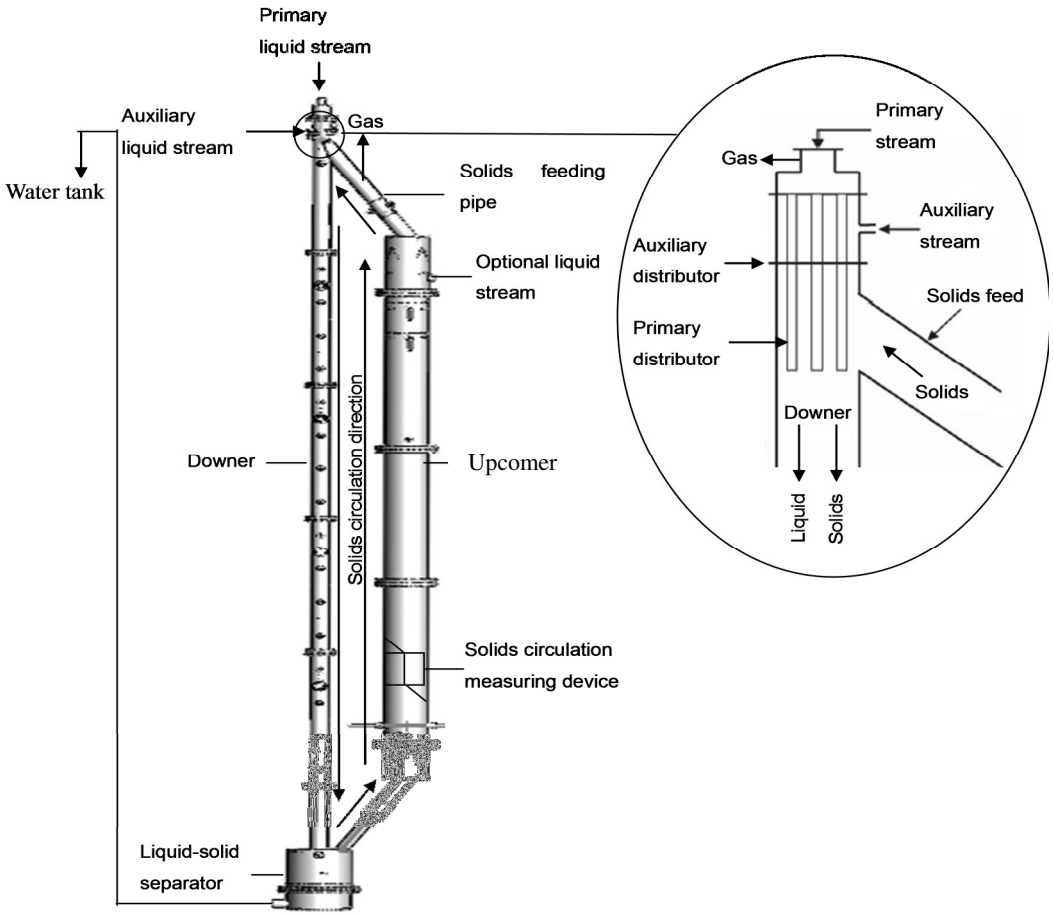

Figure 4-1: Schematic diagram of the inverse LSCFB reactor designed by Sang [15]

4.3 Results and Discussion

When the superficial liquid velocity in the downer is higher than the terminal velocity of the particles (but oppositely directed), the stream of liquid introduced from the main and auxiliary distributors carries particles in the downward direction. At the same time, particles were fed to the top of the downer by controlling the auxiliary flowrate to reach the continuous circulation of the particles in the entire system. For each operation condition tested, enough time was given to ensure the steady operation.

Figure 4-2 shows the radial particle distribution at a distance 2.1 meters below the distributor. It is clear that the distribution of the particles in radial direction is not uniform. It was observed that the distribution of the particles decreased from the central regions to the wall.

In addition, the probe was traversed in two opposite directions from the center to the wall and conversely to ensure that results are reproducible in the downer at a constant operating condition. From Figure 4-2, it is clear that traversing the probe did not influence significantly the patterns of the two-phase flow and same decreasing trend was observed.

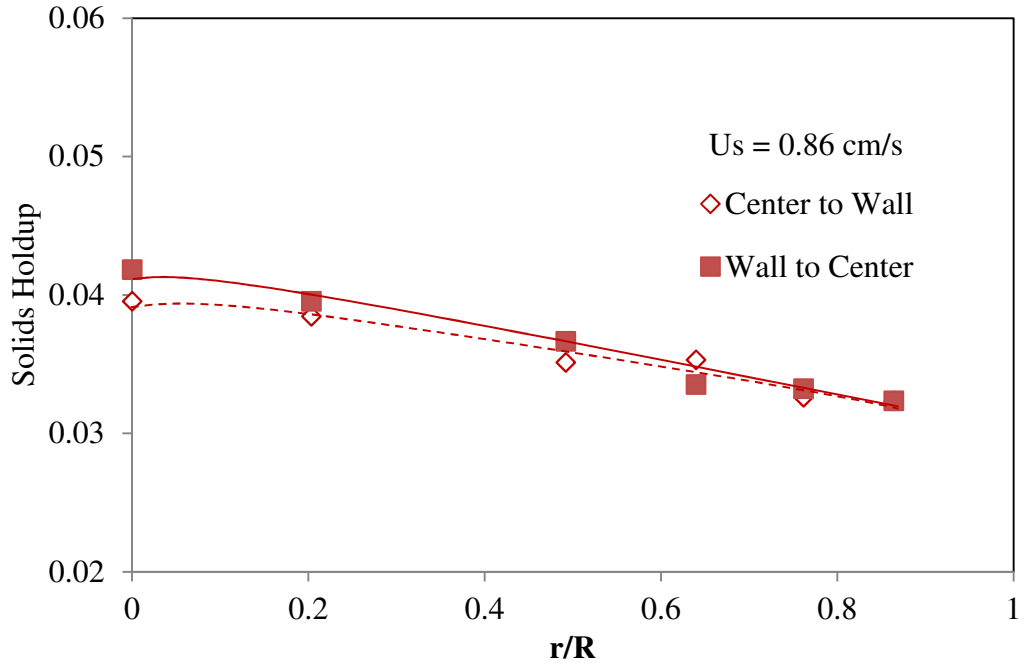

Figure 4-2: Radial distribution of the solids holdup obtained by OFP based on the comparison of the probe movement at superficial liquid velocity of U_l = 40.4 cm/s and height of 2.1 meters below the distributor

The radial profile of the solids holdup at two different axial locations under the same operating conditions was obtained by OFP in the downer and is shown in Figure 4-3. Although there was a slight difference between the values of solids holdup, a similar flow structure was observed at both locations. Again it was observed that solids holdup was higher in the central regions but lower near the wall. However, the decreasing trend at high and low superficial liquid velocities was different which is clear in both heights. For example, at superficial liquid velocity of $U_l = 22.3\ cm/s$, the solids holdup was almost constant at the central region of the column, but it decreased after reaching the point of $\frac{r}{R} = 0.640$ and this decrease continued until reaching the wall. On the other hand, at the superficial liquid velocity of $U_l = 33.4\ cm/s$, the decrease started at $\frac{r}{R} = 0.2034$ and this decrease continued until reaching the wall.

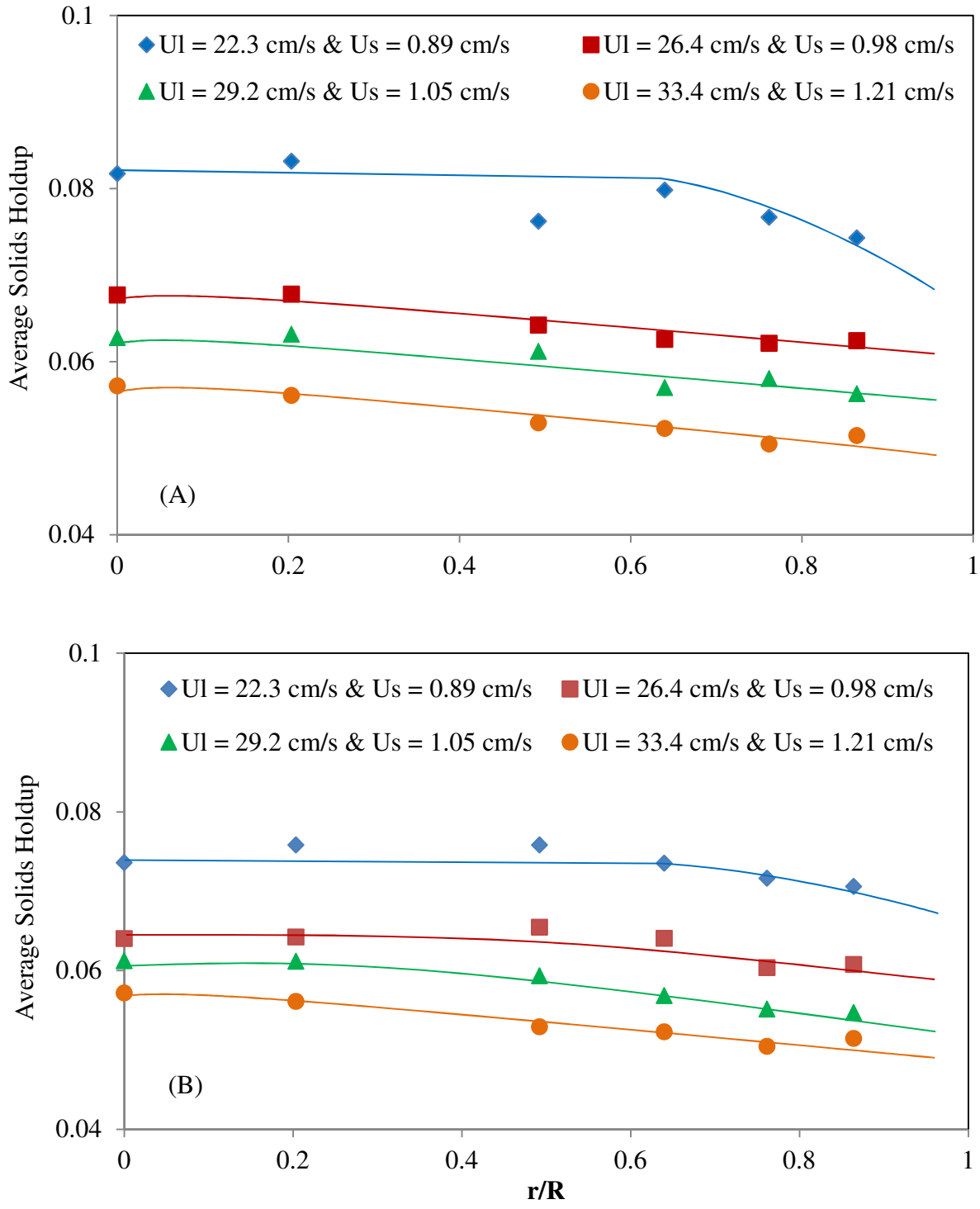

Figure 4-3: Radial distribution of the solids holdup obtained by OFP at auxiliary velocity of U_a = 5.6 cm/s and (A) height of 2.1 meters (B) height of 3.4 meters below the distributor

Figure 4-4 shows the radial distribution of solids holdup in the downer obtained by both ERT and OFP at auxiliary velocity of $U_a = 2.8\ cm/s$. Optical fiber probe was used at the location, 2.1 meters below the distributor while ERT measured the solids holdup at the location, 4.4 meters below the distributor. There was a good agreement between the both methods of measurements. However, ERT showed decreasing trends slightly different from the results obtained by the optical fiber probe. Regarding the results obtained by ERT, the central regions of the column had constant solids holdup and the decrease began after $\frac{r}{R} = 0.6396$ while a continuous decrease was observed by the OFP from the center of the pipe to the wall. One similarity between the results presented in Figures 4-3 and 4-4 is that the reduction ratio of solids holdup from center to the wall was more evident at higher velocities.

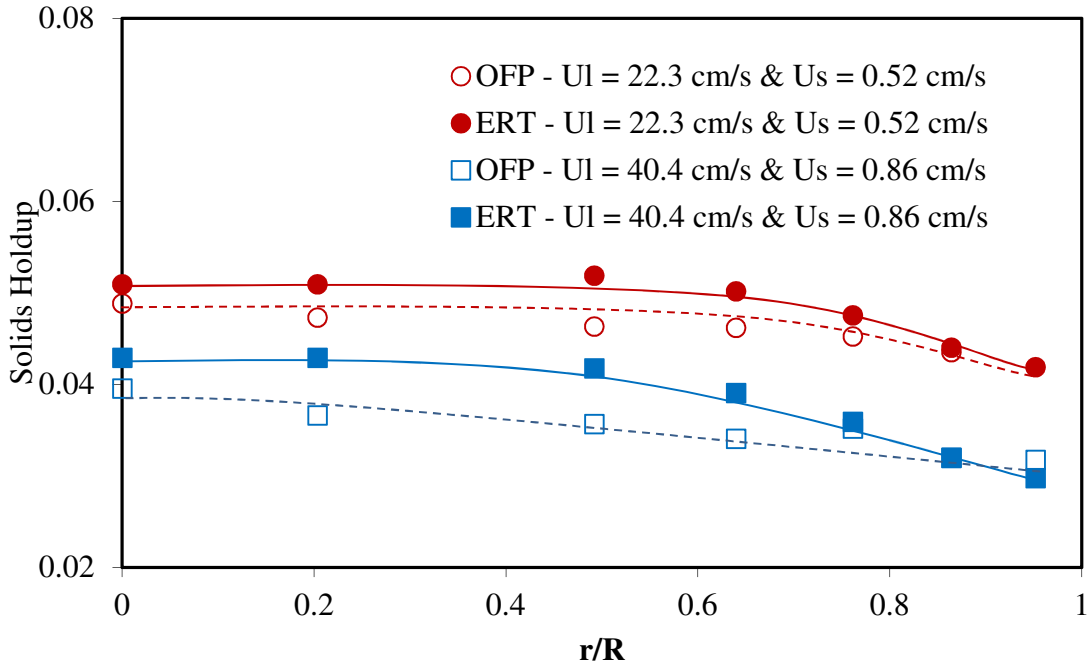

Figure 4-4: Radial distribution of the solids holdup obtained by both ERT and OFP under the two different superficial velocities at auxiliary velocity of $U_a = 2.8\ cm/s$

Figure 4-5 shows the radial distribution of the particles in the riser of the LSCFB obtained by both ERT and optical fiber probe under different superficial liquid velocities [18]. These results were obtained for glass beads with density of $\rho_s = 2500\, kg/m^3$ while the liquid was tap water. As it can be seen in Figure 4-5, solids holdup was nearly constant in the central region while it increased near the wall and the maximum amount of solids holdup was obtained near the wall. Similar two-phase radial structure had been reported by Liang et al. [16] and Zheng et al. [17] in the riser of upward LSCFB as well. According to the previous reports, it was explained that the profile of the liquid velocity is not uniform because of shear stress at the wall. Consequently higher liquid velocity in the central regions led to different distribution of drag force on particles. Since the drag force on particles near the wall region is lower, particles have higher retention time in comparison with particles in the central region. Thus, higher concentration of particles was observed at the regions near the wall.

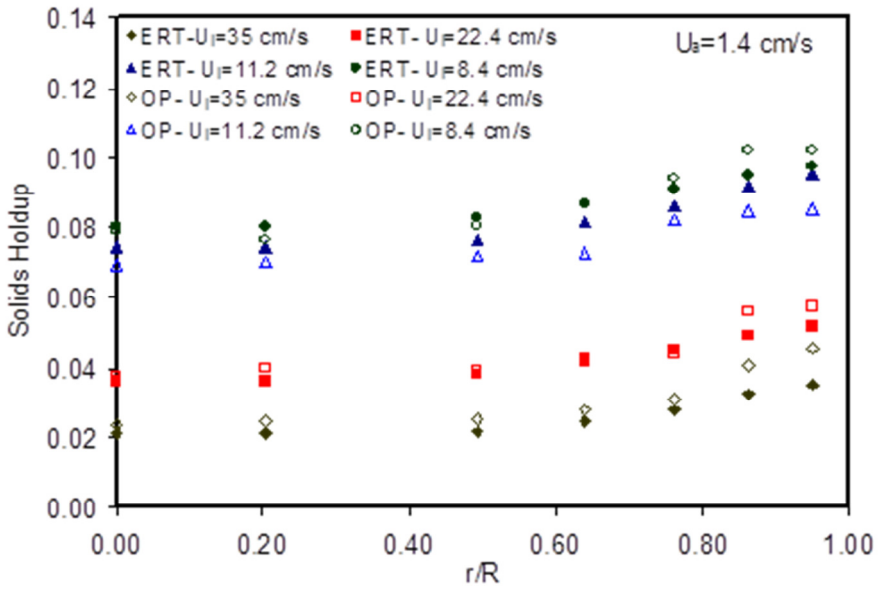

Figure 4-5: Radial distribution of the solids (glass beads) holdup using both ERT and optical fiber probe under different superficial liquid velocities at auxiliary liquid velocity of 1.4 cm/s (Razzak et al. [18])

In this study for the inverse LSCFB, lower solids holdup was observed in the wall region than central regions.

The difference in the radial particle distribution between the ILSCFB and the LSCFB can be explained by the difference in the particle-turbulence interactions of the light and heavy particles.

The radial flow structure for both inverse and upward LSCFB were tested in a column with an inner diameter of $D = 7.62\ cm$ and at total liquid velocities higher than 20 cm/s ($U_l > 20\ cm/s$). Furthermore, the solids holdup for both results did not exceed ten percent and the continuous phase was tap water. Zheng et al. [20] explained that the regime of the flow was turbulent in the riser and the existence of eddies were reported regarding the movement of the particles near the wall. In this study, erratic movement of the particles was also detected by visual observation near the wall which could show the presence of eddies as a structure of the flow. In addition, at Reynolds numbers higher than 15200, the flow regime inside the column was undoubtedly turbulent. On this basis, it is expected that turbulent eddies were present in the whole column and vortices with different intensities were exist in the column.

The particle distribution in turbulent liquid-solid flow has been studied both theoretically and experimentally. For example, Fouxon [21] found that particles with density greater than that of the liquid tend to accumulate in the regions with less vorticity while lighter particles are captured in the regions with more vorticity. Davila and Hunt [22] found out that if the ratio of particles to liquid density is lower or greater than one, particles are accelerated toward or away from the vortices respectively. Squires and Eaton [23] found out that in a turbulent two-phase flow, the regions with high solids distribution are linked to regions with less vorticity.

As a matter of fact, the vortices formed in the turbulent flow are positioned streamwise and their intensity depends on the velocity of the liquid. Thus, in the regions of the column where the liquid velocity is higher, there is a greater chance of formation of the main vorticity rather than in regions of the column where liquid velocity is lower. Actually, the liquid velocity profile is not radially uniform. Due to shear stress at the wall, liquid velocity is lower in regions near the wall and consequently regions near the wall have less vorticity rather than central regions. The above facts and the studies

reported by Fouxon [21] and Davila and Hunt [22] could be used to explain the difference between the radial particle distribution of light and heavy particles in inverse and upward LSCFB respectively. In inverse LSCFB, solids holdup was lower in regions near the wall because the intensity of the turbulent eddies is lower and particles accelerated toward the regions with more vorticity (central regions). In contrast, opposite trend of the particle distribution was observed in upward LSCFB and particles accelerated to the regions near the wall including less vorticity.

Figure 4-6 shows the three dimensional topographic view of the cross-sectional solids holdup at superficial liquid velocity of $U_l = 33.4\ cm/s$. Based on Figure 4-6, it is clear that solids holdup was higher near the central regions and decreased toward the wall regions.

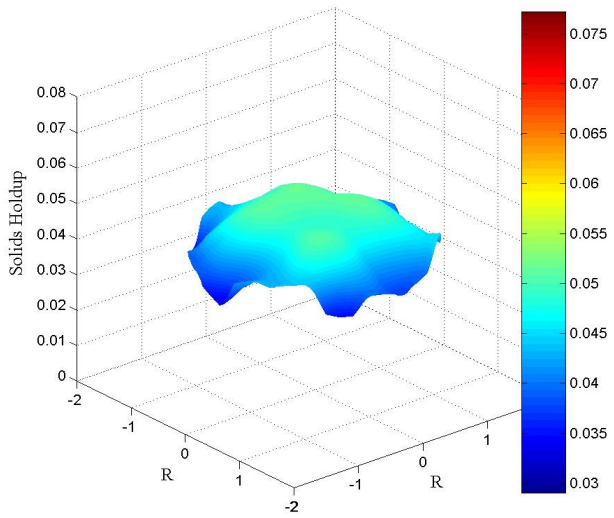

Figure 4-6: Three dimensional topographic view of the cross-sectional solid holdup at superficial liquid velocity of $U_l = 33.4\ cm/s$ and superficial solids velocity of $U_s = 1.5\ cm/s$

In order to see the distribution of the particles, the time map from the cross-sectional area of the downer was taken for 10 seconds. From the two-dimensional topography showed

in Figure 4-7, it is obvious that concentration of the particles is higher in the central region. However, a specific trend of the distribution of the particles in the central regions was not observed.

One key parameter to analyze the characteristic of the two-phase turbulent flow is the ratio of the particles diameter to a turbulence length scale [24]. The turbulent length scale is the size of the large eddies that contain the energy in turbulent flow. In a fully developed pipe flow, turbulent length scale is around 0.039 times the hydraulic diameter ($l = 0.039D$). Regarding the size of the particles used in this study, the ratio of the particles diameter (0.8 mm) to a turbulent length scale (3mm) is small. Based on the explanation of Gore and Crowe [24], it can be assumed that particles followed turbulent fluid motions.

As it is clear in Figure 4-7, the solids holdup in the central regions has been varying randomly in time. This behavior could be due to the turbulent flow of fluid, leading to random motion of particles. On this basis, distribution of the particles in the central regions seemed to vary randomly within certain limits, which shows the complicated hydrodynamic behavior of two-phase flow in the downer. However, which was clear based on the different results is that the solids holdup is greater in the central region compared to the region near the wall.

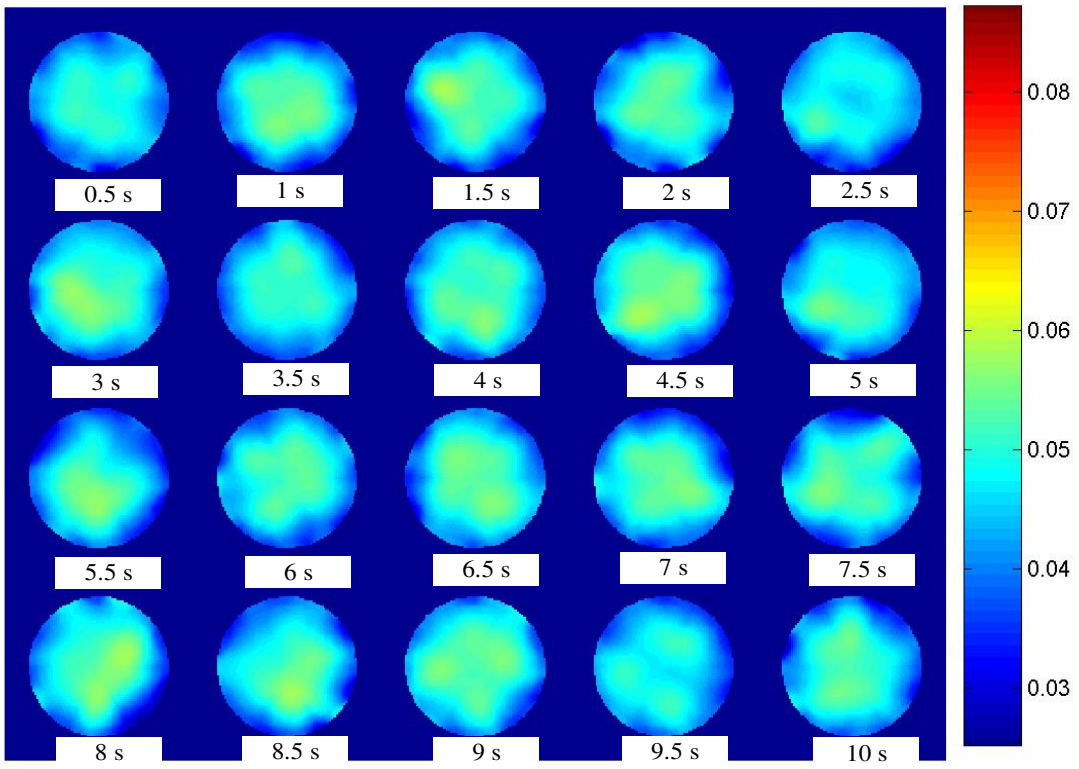

Figure 4-7: Two-dimensional topography view from 0.5s to 10s frame cross-sectional solids holdup at superficial liquid velocity of $U_l = 33.4\ cm/s$ and superficial solids velocity of $U_s = 1.5\ cm/s$

4.4 Conclusions

Phase distribution in the downer of an inverse LSCFB reactor containing particles with density lower than liquid density was studied. This novel reactor was operated at different liquid velocities and solids circulation rates and the radial distribution of the particles in the downer was measured by optical fiber probe and ERT. In this study, an unexpected radial structure of the two-phase flow was observed which was different from the case of the heavy-particle LSCFB. Similarly to the upward LSCFB, a non-uniformity of the radial particle holdup was observed in the main column. However, the radial function

was completely opposite in the two cases: the particle holdup was maximum in the center of the ILSCFB, while it was minimum in the central region of the LSCFB.

Under different liquid velocities it was observed that the decreasing trend of solids holdup from the center to the wall was more visible at higher superficial liquid velocities. This study is important not only for the further research of the inverse LSCFB but also due to very low particle density can be used to explain the gas-liquid hydrodynamic of bubble columns.

Nomenclature

D Diameter of the column (m)

U_s Superficial solids velocity (m/s)

U_a Auxiliary liquid velocity (solids-free basis) – downer (m/s)

U_l Total liquid velocity (solids-free basis) – downer (m/s)

Greek Letters

ρ_l Density of the liquid (kg/m^3)

ρ_s Density of the solids (kg/m^3)

ε_s Solids holdup

References

[1] Zhu, J.-X., D. G. Karamanev, A. S. Bassi and Y. Zheng (2000). "(Gas-) liquid-solid circulating fluidized beds and their potential applications to bioreactor engineering". The Canadian Journal of Chemical Engineering 78(1): 82-94.

[2] Chowdhury, N., J. Zhu, G. Nakhla, A. Patel and M. Islam (2009). "A novel liquid-solid circulating fluidized-bed bioreactor for biological nutrient removal from municipal wastewater". Chemical Engineering and Technology 32(3): 364-372.

[3] Lan, Q., J. X. Zhu, A. S. Bassi, A. Margaritis, Y. Zheng and G. E. Rowe (2001). "Continuous protein recovery using a liquid-solid circulating fluidized bed ion exchange system: Modelling and experimental studies". Canadian Journal of Chemical Engineering 79(4): 687-687.

[4] Patel, M., A. S. Bassi, J. J. X. Zhu and H. Gomaa (2008). "Investigation of a dual-particle liquid-solid circulating fluidized bed bioreactor for extractive fermentation of lactic acid". Biotechnology Progress 24(4): 821-831.

[5] Trivedi, U., A. Bassi, J. Zhu (2006). "Continuous enzymatic polymerizationof phenol in a liquid-solid circulating fluidized bed". Powder Technology 169(2): 61–70.

[6] Sowmeyan, R. and G. Swaminathan (2008). "Performance of inverse anaerobic fluidized bed reactor for treating high strength organic wastewater during start-up phase". Bioresource Technology 99(14): 6280-6284.

[7] Karamanev, D. G. and L. N. Nikolov (1988). "Influence of some physicochemical parameters on bacterial activity of biofilm: Ferrous iron oxidation by Thiobacillus ferrooxidans". Biotechnol Bioeng. 31(4):295-9

[8] Ramsay, B. A., D. Wang, C. Chavarie, D. Rouleau, J. A. Ramsay (1991). "Penicillin production in an inverse fluidized bed bioreactor" Journal of Fermentation and Bioengineering, Volume 72(6): 495–497

[9] Nikolov, L., D. Karamanev, T. Penev, and D. Dimitrov (1990). "Full-Scale Inverse Fluidized Bed Biofilm Reactor for Wastewater Treatment" 2nd Int. Biotechnol. Conf.: Asian-Pacific Biotechnol. Conf., 112, Seoul, Korea.

[10] Karamanev, D. G. and L. N. Nikolov (1996). "Application of inverse fluidization in wastewater treatment: From laboratory to full-scale bioreactor". Environmental Progress 15(3): 194-196

[11] Fan, L.-S., K. Muroyama and S. H. Chern (1982). "Hydrodynamic Characteristics of Inverse Fluidization in Liquid-Solid and Gas-Liquid-Solid Systems". The Chemical Engineering Journal 24(2): 143-150.

[12] Karamanev, D. G. and L. N. Nikolov (1992b). "Bed expansion of liquid–solid inverse fluidization". AICHE Journal 38(12): 1916–1922

[13] Karamanev, D. G., C. Chavarie, and R.C. Mayer (1996). "Dynamics of the free rise of light solid sphere in liquid". AICHE Journal 42(6): 1789-1792.

[14] Nikov, I. and D. Karamanev (1992). "Liquid-Solid Mass Transfer in Inverse Fluidized Bed". AICHE Journal 37(5): 781-784.

[15] Long Sang (2013). "Particle Fluidization in Upward and Inverse Liquid-Solid Circulating Fluidized Bed". The University of Western Ontario, PhD Thesis.

[16] Liang, W., J.-X. Zhu, Y. Jin, Z.-Q. Yu, Z.-W. Wang, J. Zhou (1996). "Radial non-uniformity of flow structure in a liquid–solid circulating fluidized bed". Chemical Engineering Science 51, 2001–2010.

[17] Zheng, Y., J.-X. Zhu, N. S. Marwaha and A. S. Bassi (2002). "Radial solids flow structure in a liquid-solids circulating fluidized bed". Chemical Engineering Journal 88(1-3): 141-150.

[18] Razzak, S. A., S. Barghi, J.-X. Zhu (2009). "Application of electrical resistance tomography on liquid–solid two-phase flow characterization in an LSCFB riser". Chemical Engineering Science 64(12): 2851-2858

[19] Razzak, S. A., Barghi, S., Zhu, J.-X. (2007). "Electrical resistance tomography for flow characterization of a gas–liquid–solid three-phase circulating fluidized bed". Chemical Engineering Science 62(24): 7253–7263.

[20] Zheng, Y., J.-X. Zhu, J. Wen, S. A. Martin, A. S. Bassi and A. Margaritis (1999). "The axial hydrodynamic behavior in a liquid-solid circulating fluidized bed". Canadian Journal of Chemical Engineering 51(50): 16242-16250

[21] Fouxon, I (2011). "Distribution of particles and bubbles in turbulence at small Stokes number". Physical Review Letters 108(13), Article Number: 134502

[22] Davila, J. and J. C. R. Hunt (2000). "Settling of small particles near vortices and in turbulence". J. Fluid Mech. 440, 117-145

[23] Squires, K.D. and Eaton, J.K. (1990). "Particle response and turbulence modification in isotropic turbulence". Phys. Fluids, 2(7): 1191-1203.

[24] Gore, R.A. and Crowe, C.T. (1989). "The effect of particle size on modulating turbulent intensity". Int. J. Multiphase Flow, 15, 279-285.

Chapter 5

5 Hydrodynamic characteristics of inverse liquid-solid fluidization in a large column

5.1 Introduction

One important characteristic of the inverse LSCFB system is that it is operated in two distinct regimes: the circulating fluidization regime in the downer and the conventional fluidization regime in the upcomer. These two different operating regimes have benefited the upward LSCFB reactors in different applications. In the case of the continuous protein recovery [1], a continuous circulation of the ion exchanger particles were obtained in the upward LSCFB system. In that case, the adsorption (under the circulating fluidization regime) and desorption (under the conventional fluidization regime) of proteins were carried out in the downcomer and the riser respectively. In the field of the waste water treatment [2], the riser was operated under the circulating fluidization regime in which denitrification and phosphorus release were the main reactions. On the other hand, organic oxidation and excess phosphorus uptake were the main reactions in the downcomer, operated under the conventional fluidization regime.

In addition, in the field of bioengineering, applications of inverse fluidized bed bioreactors under the conventional fluidization regime have showed different advantages such as high rate of mass transfer [3] and efficient control of biofilm thickness [4]. On this basis, more research is essential to understand further the characteristics of the inverse fluidized bed under the conventional fluidization regime.

In the past two decades, some studies of the hydrodynamic characteristics of inverse liquid-solid fluidized bed systems have been carried out. Karamanev and Nikolov [5] found that free-rising particles do not obey Newton's law for free-settling particles. Therefore, in order to measure the drag coefficient, the new correlation based on different ranges of particles density and particles Reynolds number was proposed by them. Calderon et al. [6] compared experimental data obtained in an inverse fluidized bed bioreactor to some correlations predicting bed expansion. They concluded that, the

experimental results for the terminal velocity of particles were not comparable with results obtained by correlations when drag coefficient was determined by standard drag law for free falling particles. In addition, mathematical models could not predict the experimental data when they used drag law for free rising particles proposed by Karamanev and Nikolov [5]. Some other experimental and mathematical modeling works such as flow regimes and pressure drops across the bed [7] and prediction of the experimental data based on the new correlations as a function of voidage-velocity relationship and drag force [8] were performed in the area of the inverse liquid-solid fluidization.

The aim of this work is to study hydrodynamic characteristics of conventional fluidization regime in an inverse liquid-solid fluidized bed system. For the first time, conventional fluidization regime is studied in a column with a large diameter (20 cm). The pressure drop across the bed and the bed expansion were measured experimentally and based on these measurements the minimum fluidization velocity was obtained. Then, the minimum fluidization velocity obtained experimentally was compared by mathematical correlations.

Since mathematical models were used to validate the experimental data, the Richardson and Zaki model and some important correlations for the prediction of the minimum fluidization velocity are employed.

5.2 Mathematical models of bed expansion and the minimum fluidization velocity correlation

5.2.1 Richardson and Zaki model

One of the best models to describe the hydrodynamic characteristic of the liquid-solid fluidization is the Richardson and Zaki model [9]:

$$\varepsilon^n = \frac{U_l}{U_i} \tag{5.1}$$

where the expansion index (n) is a function of the particle terminal Reynolds number (Re_t) , the particle diameter and the column diameter. The expansion index (n) is obtained by the following correlations:

$$n = \left(4.4 + 18\frac{d_p}{D}\right) {Re_t}^{-0.1} \qquad for \;\; 1 < Re_t < 200 \tag{5.2a}$$

$$n = 4.4 {Re_t}^{-0.1} \qquad for \;\; 200 < Re_t < 500 \tag{5.2b}$$

$$n = 2.4 \qquad for \;\; Re_t > 500 \tag{5.2c}$$

In addition, in Equation (5.1) U_i is the superficial liquid velocity where the bed voidage is equal to one. U_i is obtained by the following equation proposed by Richardson [10]:

$$logU_i = logU_t - \frac{d_p}{D} \tag{5.3}$$

where U_t is the terminal particle velocity and can be calculated by the following equation (Denn [11]):

$$U_t = \sqrt{\frac{4(\rho_l - \rho_s) g d_p}{3\rho_l C_d}} \tag{5.4}$$

In order to obtain C_d, Karamanev [12] proposed that for particles with $\rho_s \ll \rho_l$, the transition from the standard drag curve to $C_d = 0.95$ corresponded to $Ar = 13000$. On this basis, when the Archimedes number is higher than 13000, the drag coefficient is equal to 0.95 and when the Archimeds number was lower than $Ar = 13000$, the drag coefficient can be calculated by the following equation:

$$C_d = \frac{432}{Ar}\left(1 - 0.0470 Ar^{\frac{2}{3}}\right) + \frac{0.517}{1 + 154 Ar^{-1/3}} \tag{5.5}$$

It should be mentioned that this model is valid for particles with $\rho_s \ll \rho_l$ similar to this study.

5.2.2 The minimum fluidization velocity

The minimum fluidization velocity is an important hydrodynamic parameter because it demonstrates the beginning of the fluidization and demarcates the conventional fluidization regime from the fixed bed state. The minimum fluidization Reynolds number is defined by the following equation:

$$Re_{mf} = (C_1^2 + C_2 Ar)^{0.5} - C_1 \tag{5.6}$$

where $C_1 = \frac{1}{\varepsilon_{mf}^3 \varphi_s}$ and $C_2 = \frac{1-\varepsilon_{mf}}{\varepsilon_{mf}^3 \varphi_s}$

One difficulty in using the above correlation is in determination of the shape factor and bed voidage. Lucas et al. [13] classified the particles in three categories according to their shapes and by obtaining the optimum values of C_1 and C_2, proposed one equation for each category. In addition, in their study most important equations of the minimum fluidization Reynolds number were presented. This is discussed in the results and discussion section.

5.3 Experimental Setup

All experiments were carried out in the upcomer (riser) having a diameter of 20 cm. The liquid phase was tap water and it was introduced from the top of the column (shown in Figure 5-1). In order to maintain the continuous recirculation of water as a continuous phase, the water which exited the bottom of the upcomer was flown to the water tank through the pipe connected to the separator (Figure 5-1). This pipe had a Π – shape. The maximum height of the pipe was located at the highest point of the system to ensure that the entire system was filled with water during the experiments.

The solid phase was represented by spherical Styrofoam beads with a mean diameter of 0.8 mm and a density of 28 kg/m^3. The density of particles was measured by a fully automatic and accurate gas displacement pycnometer, AccuPyc 1340. All experiments were performed at ambient temperature.

Six ports at different heights were placed along the upcomer and connected to the six manometers. The measurement procedures of the bed expansion and the frictional bed pressure drop were explained in chapter 2.

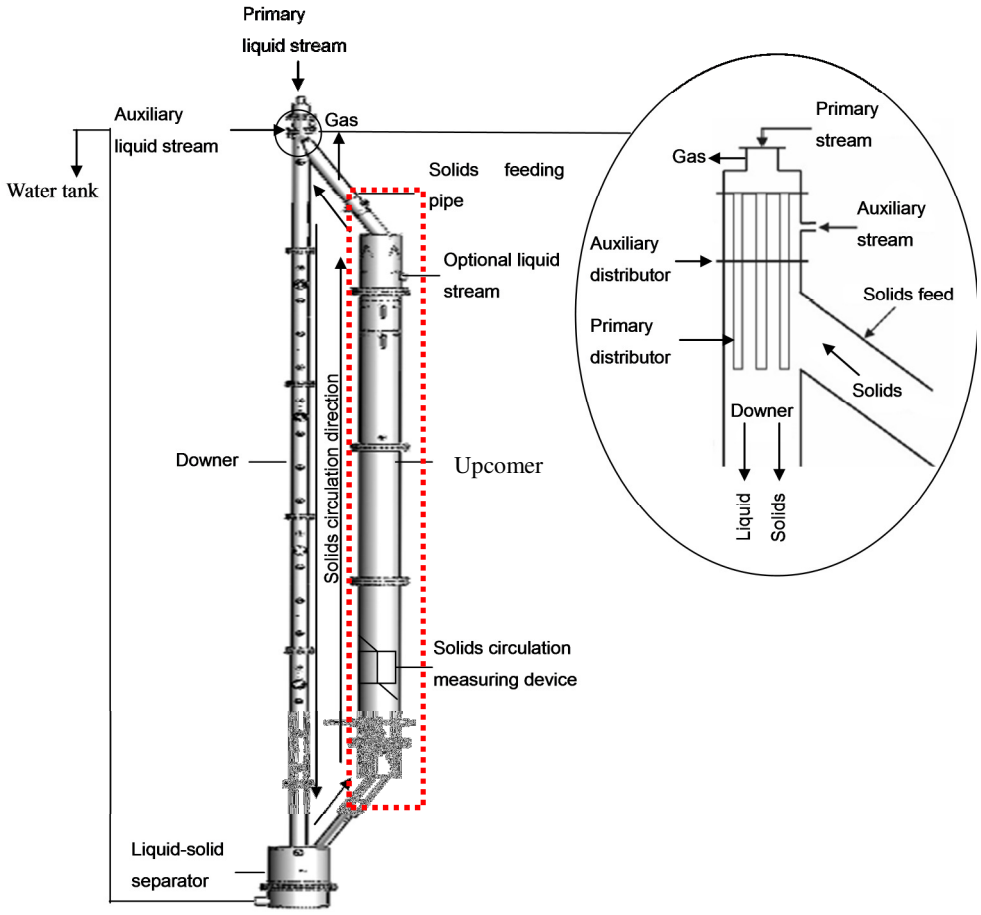

Figure 5-1: Schematic diagram of Inverse LSFB reactor designed by Sang [15]

5.4 Results and discussions

Figure 5-2-A shows the variation of the frictional bed pressure drop across the entire bed as a function of the superficial liquid velocity in the upcomer. It is clear that below the minimum fluidization velocity, the frictional bed pressure drop increased when the superficial liquid velocity increased. Beyond the minimum fluidization velocity, by increasing the superficial liquid velocity, the frictional bed pressure drop increased insignificantly.

Based on Figure 5-2, the variation of the frictional bed pressure drop versus the superficial liquid velocity in the upcomer was obtained under two different conditions. Under the first condition, the entire system had no solids circulation ($U_s = 0\ cm/s$) and the variation of the frictional bed pressure drop was measured versus the superficial liquid velocity. Consequently, the minimum fluidization velocity was determined from the superficial liquid velocity at which a sharp change in the frictional pressure drop occurred. On the other hand, when the entire system was under the solids circulation mode ($U_s = 1.4\frac{cm}{s}$ in the downer and $U_s = 0.2\ cm/s$ in the upcomer), the same trend was observed for the variation of the frictional bed pressure drop versus the superficial liquid velocity. In this condition, the pressure drop across the bed was higher in comparison to the condition in which the entire system was not in the solids circulation mode. Since the system faced an unstable operation, the pressure drop across the bed was not obtained at higher liquid flowrates in the upcomer. Actually, the liquid stream introduced from the top of the upcomer was conducted at the bottom of the upcomer into the return pipe and then the separator. This stream created the resistance for particles moving from the separator to the upcomer. On this basis, particles entered the downer, but they could not leave it and the system was unstable.

However, it was expected that the minimum fluidization velocity of particles in the upcomer at solids circulation mode was achieved at a superficial liquid velocity of $U_{mf(Ur\neq0)} = U_{mf(Ur=0)} + U_s$. (It should be mentioned that U_s is the superficial solids velocity in the upcomer and $U_{mf(Ur=0)}$ is the minimum fluidization velocity of particles when the system is not in the mode of the solids circulation.)

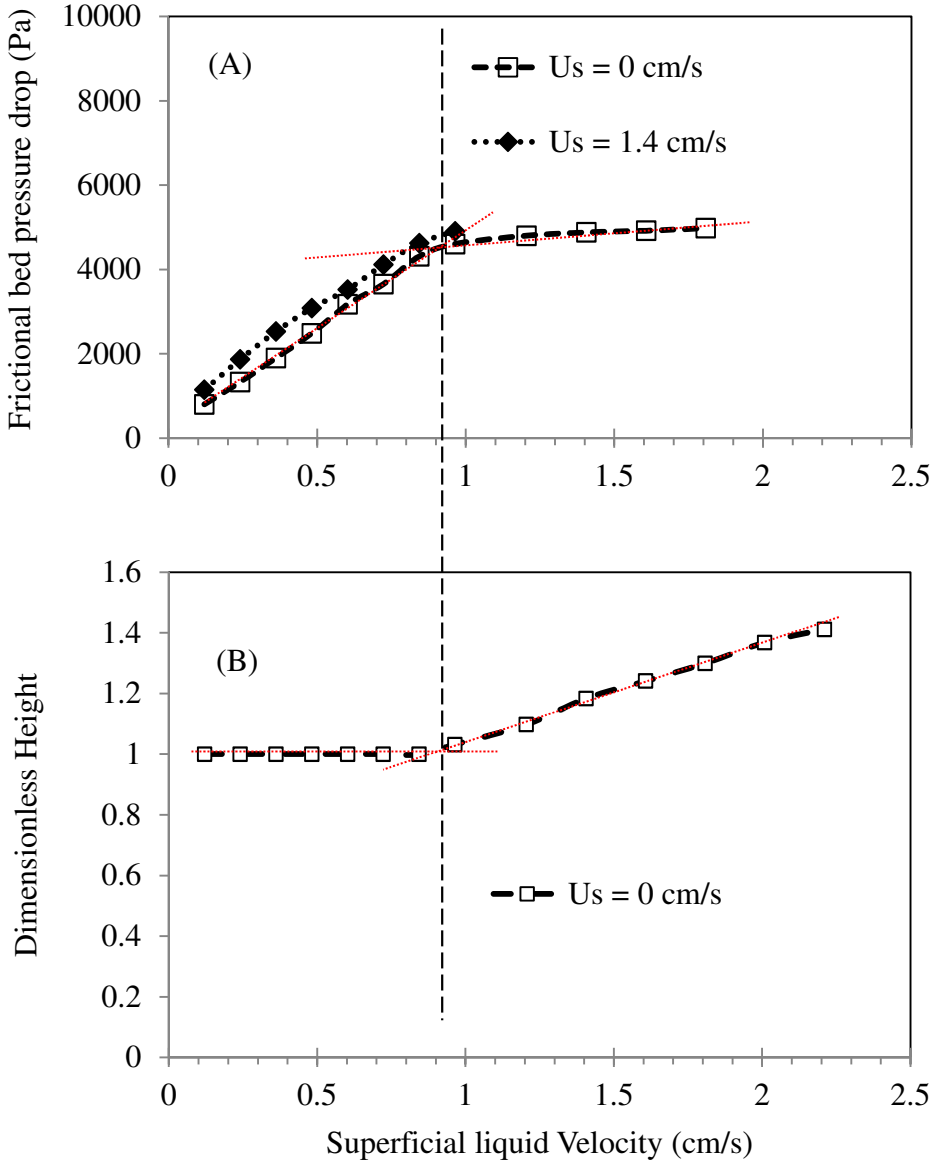

Figure 5-2: Variation of (A) the frictional bed pressure drop (B) the dimensionless height versus the superficial liquid velocity in the upcomer

Figure 5-2-B shows the variation of the dimensionless height versus the superficial liquid velocity in the upcomer. It is clear that beyond the minimum fluidization velocity, the dimensionless height increased by increasing the superficial liquid velocity. The minimum fluidization velocity obtained based on Figure 5-2-B was in agreement with the

velocity obtained based on the variation of the pressure drop across the bed versus the superficial liquid velocity.

The experimental minimum fluidization velocity obtained in this study was compared with the Richardson and Zaki model [9] and other correlations listed in Table 5-1. Based on Table 5-1, it is clear that the minimum fluidization velocities calculated by the correlations other than the Richardson and Zaki, are not close to the velocity obtained experimentally. However, the Richardson and Zaki model could predict the minimum fluidization velocity with high accuracy. In this model, the drag coefficient for a free rising particle was used. In addition, it was found that the Richardson and Zaki model is reliable to predict the minimum fluidization velocity of particles in a column with a large diameter.

Table 5-1: The minimum fluidization velocity obtained by mathematical models and experimentally

The experimental results and mathematical models	The minimum fluidization velocity (cm/s)
Experimental Results	0.92
Richardson & Zaki model [9]	0.89
Thonglim [15] $\boldsymbol{Re_{mf} = (31.6^2 + 0.925Ar)^{0.5} - 31.6}$	0.81
Saxena and Vogel [16] $\boldsymbol{Re_{mf} = (25.25^2 + 0.0571Ar)^{0.5} - 25.28}$	0.63
Babu et al. [17] $\boldsymbol{Re_{mf} = (25.25^2 + 0.0571Ar)^{0.5} - 25.28}$	0.71

5.5 Conclusion

In this chapter, some hydrodynamic characteristics of inverse liquid-solid fluidization under the conventional fluidization regime were studied in the upcomer. The variation of the frictional bed pressure drop and the dimensionless height versus the superficial liquid velocity were obtained. The minimum fluidization velocity was also determined. It was observed that the Richardson and Zaki model is still one of the best models to predict the hydrodynamic characteristics of fluidized systems, even in a column with a large diameter. In addition, in this model the drag coefficient for a free rising particle was used.

Nomenclature

Ar	Archimedes number defined by $d^3 g(\rho_l - \rho_p)\rho_l/\mu^2$
C_1 and C_2	Coefficients in the equation of the minimum fluidization velocity
C_d	Particle drag coefficient
d_p	Particle diameter (m)
D	Column diameter (m)
g	Gravity acceleration $(\frac{m}{s^2})$
n	Exponent in Richardos and Zaki model
Re_{mf}	Minimum fluidization Reynolds number defined by $d_p U_{mf}\rho_l/\mu$
Re_t	Particle Reynolds number defined by $d_p U_t \rho_l/\mu$
U_s	Superficial Solids Velocity (m/s)
U_{mf}	Minimum fluidization Velocity (m/s)
U_t	Terminal velocity of solid particle (m/s)
U_l	Total Liquid Velocity (m/s)
U_i	The extrapolated value of U at $\varepsilon = 1$ (m/s)
U_r	Total liquid velocity (solids-free basis) in the upcomer (m/s)

Greek Letters

ρ_l	Density of the Liquid (kg/m^3)
ρ_s	Density of the Solids (kg/m^3)
ε	Liquid Holdup

References

[1] Chowdhury, N., J. Zhu, G. Nakhla, A. Patel and M. Islam (2009). "A novel liquid-solid circulating fluidized-bed bioreactor for biological nutrient removal from municipal wastewater". Chemical Engineering and Technology 32(3): 364-372.

[2] Lan, Q., J. X. Zhu, A. S. Bassi, A. Margaritis, Y. Zheng and G. E. Rowe (2001). "Continuous protein recovery using a liquid-solid circulating fluidized bed ion exchange system: Modelling and experimental studies". Canadian Journal of Chemical Engineering 79(4): 687-687.

[3] Nikov, I. and D. Karamanev (1992). "Liquid-Solid Mass Transfer in Inverse Fluidized Bed". AICHE Journal 37(5): 781-784.

[4] Karamanev, D. G. and L. N. Nikolov (1996). "Application of inverse fluidization in wastewater treatment: From laboratory to full-scale bioreactor". Environmental Progress 15(3): 194-196

[5] Karamanev, D. G. and L. N. Nikolov (1992a). "Free rising spheres do not obey Newton's law for free settling". AICHE Journal 38(11): 1843–1846.

[6] Calderon, D. G., P. Buffiere, R. Moletta, S. Elmaleh, (1998). "Influence of biomass accumulation on bed expansion characteristics of a down-flow anaerobic fluidized-bed reactor". Biotechnology and Bioengineering 57(2): 136–144.

[7] Ulaganathan, K., K. Krishnaiah (1996). "Hydrodynamic characteristics of two-phase inverse fluidized bed". Bioprocess Engineering 15(3): 159–164

[8] Fan, L.-S., K. Muroyama and S. H. Chern (1982). "Hydrodynamic Characteristics of Inverse Fluidization in Liquid-Solid and Gas-Liquid-Solid Systems". The Chemical Engineering Journal 24(2): 143-150.

[9] Richardson, J. F. and W. N. Zaki (1954). "Sedimentation and fluidization". Part 1. Transactions of the Institution of Chemical Engineers 32(1): 35-52.

[10] Richardson, J. F. (1971). "Transient Fluidization and Particulate Systems". Fluidization, J. F. Davidson and D. Harrison, eds., 39, Academic Press, New York.

[11] Denn, M. M (1980). "Process Fluid Mechanics" Prentice Hall, Englewood Cliffs, NJ

[12] Karamanev, D. G. (1996). "Equations for calculation of the terminal velocity and drag coefficient of solid spheres and gas bubbles". Chemical Engineering Communications 147, 75-84.

[13] Lucas, A., J. Arnaldos, J. Casal, and L. Pulgjaner (1986). "Improved Equation for the Calculation of Minimum Fluidization Velocity". Industrial and Engineering Chemistry Research 26(3): 633-634

[14] Long Sang (2013). "Particle Fluidization in Upward and Inverse Liquid-Solid Circulating Fluidized Bed". The University of Western Ontario, PhD Thesis.

[15] Thonglimp V. (1981). These Dr. Inggnieur. Institut National Polytechnique de Toulouse, France

[16] Saxena, S. C.; Vogel, G. J (1977). Trans. Inst. Chem. Eng. 55, 184.

[17] Babu, S. P.; Shah, B.; Talwalkar (1978). A. AICHE Symp. Ser. 74, 176.

Chapter 6

6 Conclusions and Recommendations

6.1 Conclusions

In this work, the hydrodynamic characteristics of the inverse liquid-solid circulating fluidized bed under a wide range of operating conditions were studied. In addition, the hydrodynamic behavior of the inverse liquid-solid fluidization under the conventional fluidization regime in a column with a large diameter was also studied.

In the axial hydrodynamic behavior of the inverse LSCFB, it was found that the axial distribution of particles in the downer is uniform. The axially averaged solids holdup in the downer as a function of superficial liquid velocity was similar to the results that had been obtained in the riser of the liquid-solid circulating fluidized bed containing the particles with density higher than liquid density. Two distinct zones including the initial circulating fluidization zone and fully developed circulating fluidized zone were observed which is again similar to the results obtained in the upflow liquid-solid circulating fluidized bed. Afterwards, the effect of solids inventory in the upcomer on solids circulation rate and axially averaged solids holdup in the downer was studied. It was observed that by increasing the solids inventory in the upcomer, solids circulation rate and consequently the average solids holdup in the downer were increased. Finally, a stream of liquid was introduced from the top of the upcomer to have a counter current two-phase flow in it. It was concluded that under this condition, the axial average solids holdup in the downer and solids circulation rate were almost increased two times in comparison with the condition that the flowrate of the liquid in the upcomer was set to zero.

In order to study the radial distribution of light particles in ILSCFB, two different methods of measurement were used. The electrical resistant tomography and optical fiber probe were applied as non-intrusive and intrusive techniques, respectively, to determine

the solids holdup. Based on the results, it was observed that the radial particle distribution in the downer was different from that in the corresponding riser of a liquid-solid circulating fluidized bed where the particles density was higher than the liquid density. As in the upward LSCFB, radial non-uniformity of solids holdup was observed. However, the radial distribution of solids holdup was completely opposite in the LSCFB and the ILSCFB. The solids holdup in the downward ILSCFB decreased from the central regions to the regions near the wall, as opposed to increasing in the upward LSCFB. The decreasing trend of solids holdup from the center to the wall was more pronounced at higher superficial liquid velocities.

The hydrodynamic behavior of the inverse fluidized bed in the upcomer with a large diameter was also studied. Based on the measurements of the frictional bed pressure drop and the bed expansion, the minimum fluidization velocity was obtained. It was found that the Richardson and Zaki model could predict the minimum fluidization velocity when calculating the terminal velocity; the drag law for free rising particles was used.

6.2 Recommendations

In this study, only one type of particles with a mean diameter of 0.8 mm and a density of 28 $kg/m^3$was used. However, particles with different densities, sizes and shapes should be used in future works. Axial and radial hydrodynamic characteristics of the ILSCFB system should be studied based on particle properties. In this case, conclusions obtained in this work such as axially uniform solids holdup or the radial distribution of particles can be generalized.

In this work, because of limitations of measuring systems, solids velocity was not measured. Study of particles velocity and even liquid velocity are essential to understand the radial distribution of particles.

In the mode of solids circulation, when particles were fluidized in the upcomer at high flowrates, the entire system was unstable. It is recommended that proper modifications will be considered in the design of the system and experiments will be completed.

Appendices

Appendix A: Operation of the ERT

After the calibration of ERT, The conductivity of water was kept constant. Based on Maxwell`s equation, two parameters are important for the ERT to determine the solids holdup. Firstly, the conductivity of water obtained in the last step of the calibration. Secondly the conductivity of the mixture (water and particles) was obtained during the experiments.

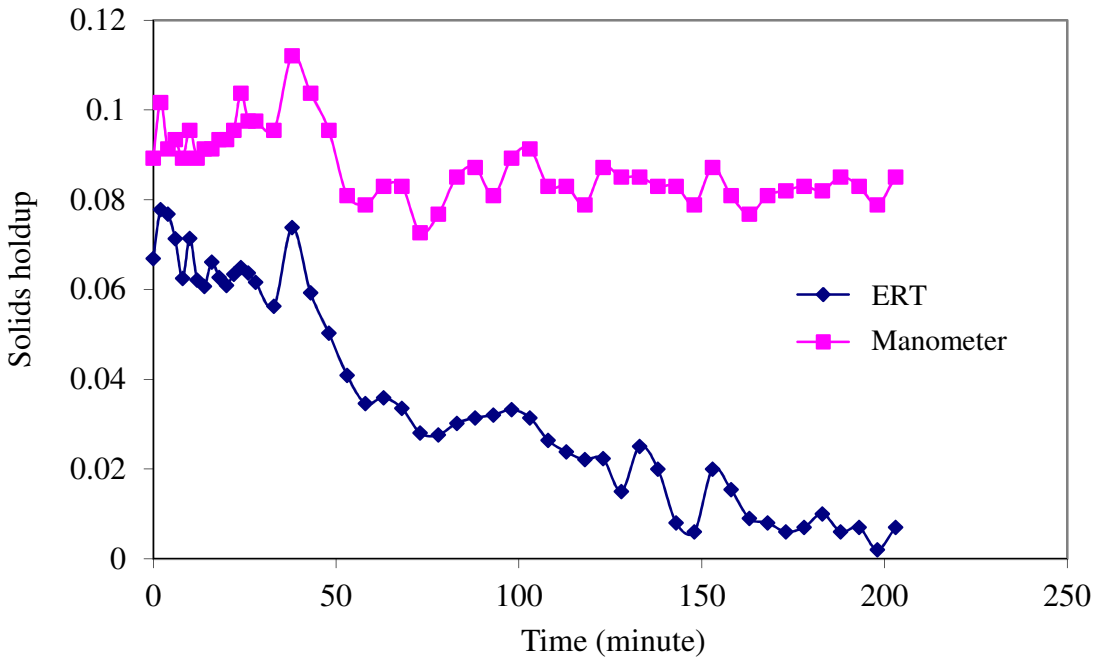

Figure A-1: Variation of the solids holdup versus time at the superficial liquid velocity of $U_l = 20.9\ cm/s$ and the superficial solids velocity of $U_s = 0.87\ cm/s$ obtained by both ERT and manometers when for each measurement by the ERT σ_m was obtained, but data was processed by the first value of σ_l measured at the last step of the calibration

After several experiments, it was found that for each flowrate when a measurement was obtained by the ERT for the mixture flow; the conductivity of the single phase liquid should also have been measured. In this case, the auxiliary valve was closed to prevent the circulation of particles and the ERT was run to take one second of data while only single phase liquid flowed through the test section. Then for this flowrate, two conductivities were processed by Maxwell`s equation. Figure 8 shows the validation of the ERT results in comparison with manometers.

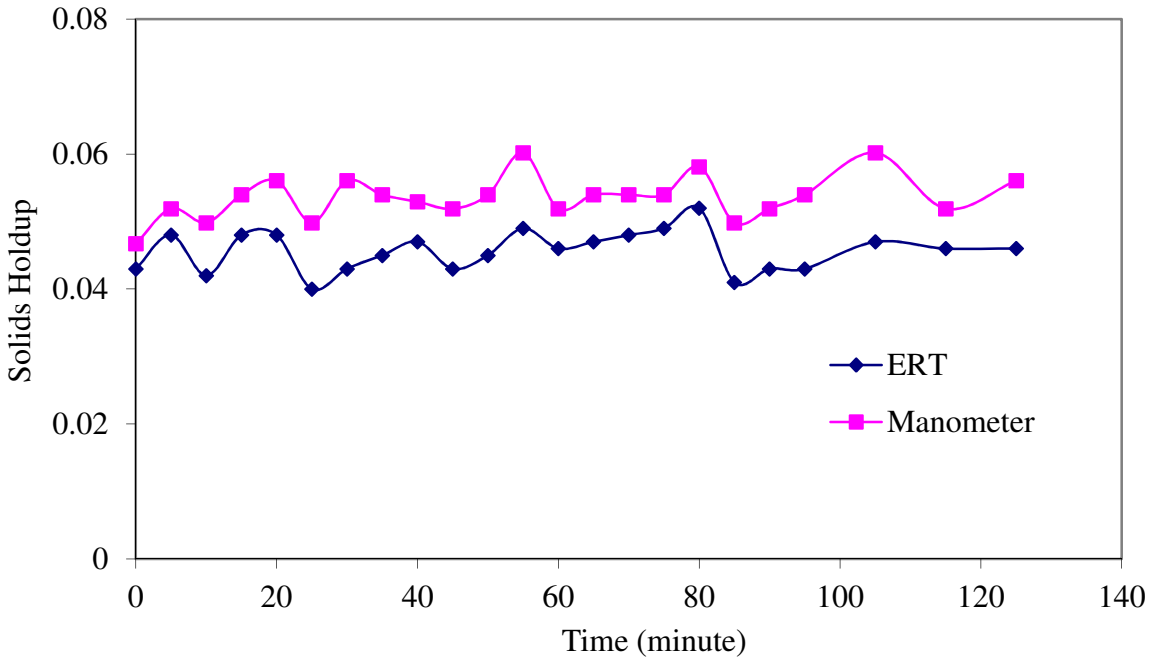

Figure A-2: Variation of the solids holdup versus time at the superficial liquid velocity of $U_l = 22.3\ cm/s$ and the superficial solids velocity of $U_s = 0.52\ cm/s$ obtained by both ERT and manometers when for each measurement σ_m and σ_l were obtained

Appendix B: An example of error bars for solid holdup

In this study, to show the accuracy of solids holdup measurements, preliminary measurements and analyses of standard error were taken at a constant auxiliary liquid velocity of $U_l = 2.8\ cm/s$ and two different liquid velocities in the downer. For each radial position 10 measurements were carried out. Figure B-1 shows an example of error bars for solid holdup.

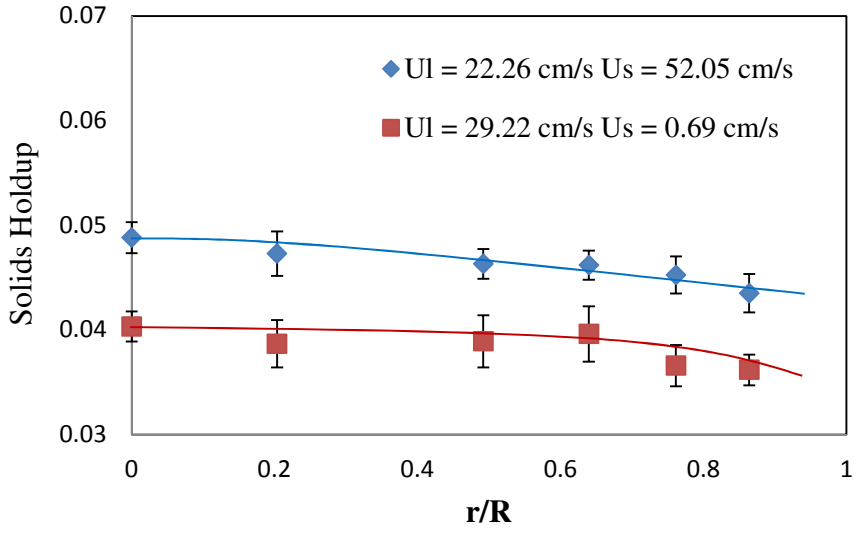

Figure B-1: Error bars for radial solid holdup

Name: Amin Jaberi

Post-secondary Education and Degrees:

Department of Mechanical Engineering
Power and Water University of Technology, Tehran, Iran
2003-2008 B.A.

Department of Mechanical Engineering
Tarbiat Modares University, Tehran, Iran
2008-2011 M.A.

Department of Chemical Engineering
The University of Western Ontario, London, Ontario, Canada
2012-2014 M.A.

Related Work Experience

Teaching Assistant
Research Assistant
The University of Western Ontario
2012-2014